UNIVERSITÀ
DEGLI STUDI
FIRENZE

DOTTORATO DI RICERCA IN
SCIENZE BIOMEDICHE

CICLO XXIX

COORDINATORE Prof. Persio Dello Sbarba

A study of the mechano-kinetic parameters of different isoforms of muscle myosin II *in vivo*

Settore Scientifico Disciplinare BIO/09

Dottorando
Dott. Percario Valentina

Tutori
Prof. Piazzesi Gabriella

Prof. Linari Marco

Coordinatore
Prof. Dello Sbarba Persio

Anni 2013/2016

Acknowledgments

Con queste poche righe vorrei ringraziare tutti i componenti del Physiolab.

In particolar modo la Prof.ssa Gabriella Piazzesi, il Prof. Marco Linari e il Prof. Vincenzo Lombardi perché grazie a loro ho capito quanto siano fondamentali per il successo di questo lavoro passione, dedizione ed entusiasmo.

Ringrazio inoltre le mie compagne di viaggio Giulia, Irene e Francesca per le tante risate e la complicità che si è creata fin dal primo momento.

Infine, mille volte grazie al Dott. Marco Caremani, il suo costante supporto (non solo scientifico) è stato per me davvero prezioso.

Index

Chapter 1 - Introduction

Skeletal muscles allow walking, running and breathing by converting chemical energy into power (force and shortening). At molecular level force and shortening are generated by cyclic interactions between the molecular motor myosin II, an ATP-driven mechanoenzyme, emerging from the thick (myosin containing) filament and organized in arrays in each half-sarcomere, and the thin (actin containing) filament, used as a track to move along. In each interaction the hydrolysis of one ATP molecule provides about 90 zJ of free energy (Pate & Cooke, 1989; Smith *et al.*, 2008), allowing the motor to exert 6 pN force and/or 6-10 nm movement (the working stroke, (Rayment *et al.*, 1993b; Piazzesi *et al.*, 2002). Thousands of half-sarcomeres in series amplify the small movement, allowing macroscopic shortening of muscle.

The performance of skeletal muscles contracting under isometric conditions or actively shortening against an external load exhibits a large variability: parameters such as speed of isometric force development, unloaded shortening velocity, maximum power output and ATPase activity vary from one muscle to the other according to their functional tasks. Muscles involved in maintenance of posture exhibit a low shortening speed at any given load, developing a lower power and consuming ATP at lower rate, with respect to muscles involved in movement that exhibit a high shortening velocity at any load, develop higher power and consume ATP at higher rate. At the same time the efficiency of energy conversion in slow muscle is similar to (Barclay *et al.*, 1993; He *et al.*, 2000) or even higher than (Woledge, 1968; Reggiani, 2007; Barclay *et al.*, 2010b) that in fast muscle. These differences are believed to be related to the myosin heavy chain (MHC) isoform expressed in different skeletal muscles (Schiaffino & Reggiani, 2011). In fact, muscles responsible for the maintenance of posture contain fibres expressing mostly the slow MHC isoform while those involved in movement contain fibres expressing mostly the fast MHC isoform. At molecular level these differences could be related either to the properties of the myosin motor *per se* (i.e. stiffness, force, size and speed of the working stroke) and/or to the properties of the ensemble of motors in the half-sarcomere (i.e. the number of motors attached to actin during an isometric or isotonic contraction and the cooperativity among motors).

In my PhD thesis high resolution mechanics has been used to investigate the differences in mechanical and kinetic properties of slow and fast myosin isoforms *in situ* during isometric and isotonic contractions. The study has been performed on single demembranated fibres isolated from soleus (containing the slow myosin isoform) and psoas (containing the fast myosin isoform) muscles of rabbit by determining (*i*) the fraction of motors attached to actin in the half-sarcomere during

isometric contraction (β), the stiffness (ε) and the force (F_0) of the motor and (*ii*) the mechanical parameters (size and speed) of the working stroke. Results show that ε of the slow myosin isoform is 1/3 of that of the fast myosin isoform. The average strain of the myosin motor during force generation (s_0) is similar (≈ 3.3 nm) in the two MHC-isoforms, indicating that the slow myosin isoform bears a force which is 1/3 of that of the fast myosin isoform. At low load the size of the working stroke is similar in slow and fast myosin while at high load is smaller in the slow isoform. On the contrary, the speed of the working stroke is one-order of magnitude slower in slow myosin at any load. The lower stiffness and lower force of the slow myosin open the question on the molecular basis of the similar/higher efficiency of slow muscle with respect to fast muscle.

In the following sections the current knowledge about the molecular mechanism of muscle contraction and the functional differences between slow and fast muscles will be briefly reviewed.

1.1 The structure of skeletal muscle

Skeletal muscle is constituted by multinucleated cells, the muscle fibres, 30-200 μm in diameter, running for the whole length of the muscle (Fig. 1A).

Under the light microscope each muscle fibre appears striated because of the regular repeat of dark bands (A-bands, anisotropic under polarised light) and light bands (I-band, isotropic under polarised light) along the myofibrils, the cylindrical units of 1 μm diameter that constitute the fibre.

Electron microscopy reveals that the bands are due to the regular repeat of two sets of interdigitating myofilaments (Fig. 1B and Fig. 2): the thin filament, mainly constituted by the protein actin (1-1.2 μm long, 8 nm in diameter) and the thick filament mainly constituted by the protein myosin (1.6 μm long, 12 nm in diameter). The thin filament originates from the Z-line, at the centre of the I-band and partially overlaps to the thick filament in the A-band. The centre of the A-band contains only thick filaments and appears less dark (H-band). The H-band is bisected by the M-line, which contains proteins connecting the thick filaments together. Two consecutive Z-lines define the sarcomere, the structural unit of the striated muscle, that repeats thousands of times along the myofibrils. Cross section of skeletal muscle reveals that thin and thick filaments are disposed in a double hexagonal lattice: in the overlap region each thick filament is surrounded by six thin filaments, while each thin filament is surrounded by three thick filaments (Fig. 1 D3) so that the ratio thick/thin filament is 1:2. Across the Z-line, the thin filaments are arranged in a tetragonal pattern: each thin filament is connected with 4 thin filaments from neighbouring sarcomeres (Fig. 1 D5).

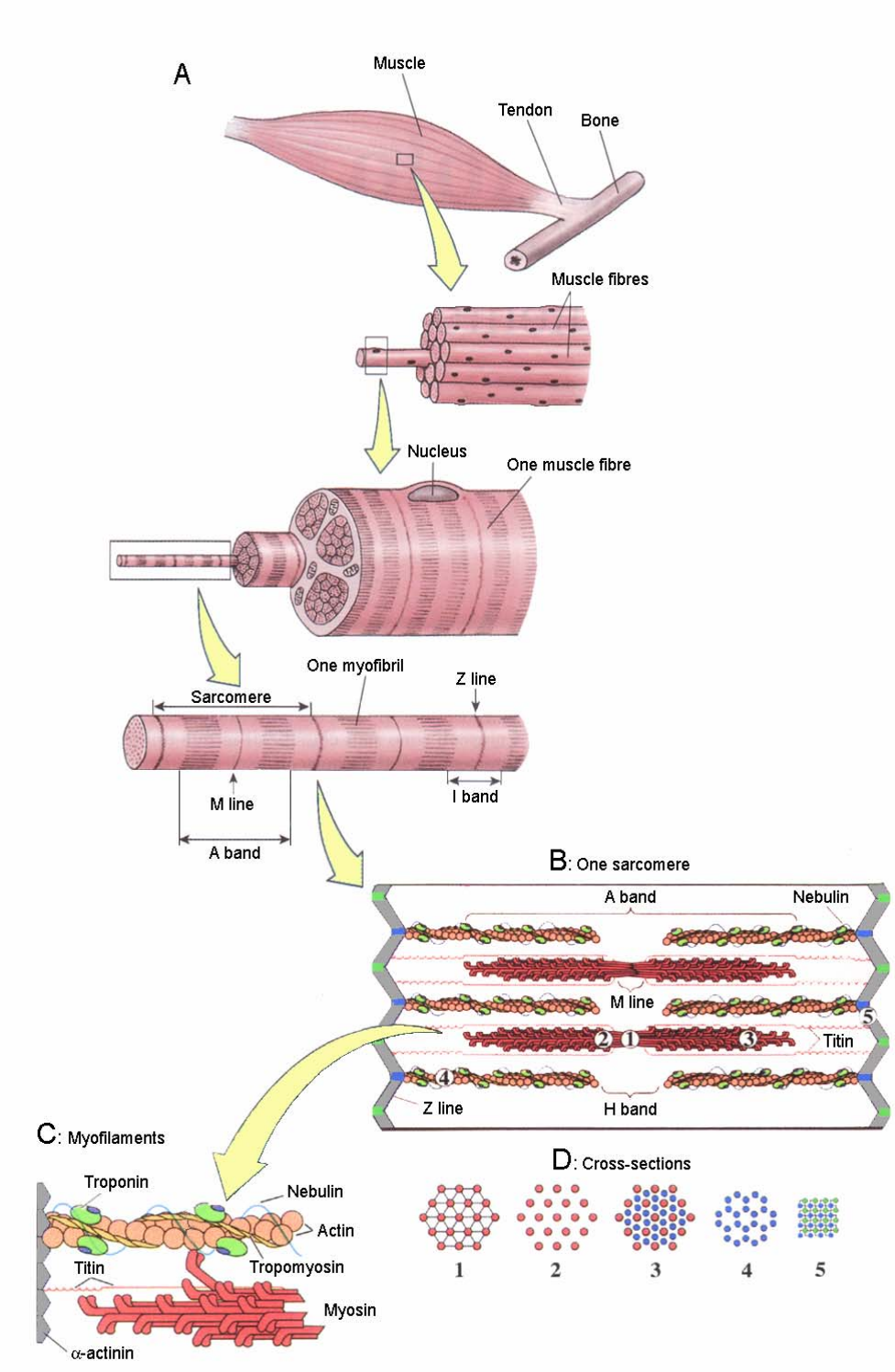

Figure 1. Muscle structure at different levels of organization. **A.** From muscle to fibres, myofibrils and sarcomere. **B.** Sarcomere structure with the interdigitation of thick (red) and thin (orange) filaments. **C.** The contractile, regulatory and structural proteins in more details. **D (1-5).** Cross sections showing the lattice organization corresponding to the numbers in B.

1.1.1 Contractile proteins

Myosin and actin are the proteins responsible for muscle contraction. Skeletal muscle myosin belongs to the family of the myosin motor class II (Sellers, 1999). The myosin molecule is an examer of 520 kDa molecular weight (Fig. 3) and consists of two heavy chains (220 kDa molecular weight) each composed of a 150 nm long 'tail' and a globular 'head' at one end, and two pairs of light chains (20 kDa molecular weight each). Partial digestion by trypsin splits the molecule in two fragments, the light meromyosin (LMM), constituted by the major part of the tail, and the heavy meromyosin (HMM) that contains the two heads and the rest of the tail. Further digestion by papain splits HMM into three sub fragments: two S1 portions, the heads, and a rod-like S2 portion. The S2 portions form a coiled-coil structure which continues in the LMM that constitutes the backbone of the thick filament. The S1 portion of the myosin monomer consists of the catalytic domain (CD), or motor domain (MD), containing the sites for actin binding and for ATP hydrolysis, and the light chain domain (LCD), an elongated portion that has the binding sites for the light chains and is connected with its carboxyl terminal to the S2 rod (Fig. 4). The primary structure of the HMM contains about 1900 amino acids of which about 840 form the S1 portion of the head. In the thick filament the myosin molecules are arranged in two antiparallel arrays, with the tails in each half of the thick filament pointing toward the centre of the sarcomere. Consequently, in the centre of the thick filaments, a region of ca 200 nm, called the bare zone, is free of heads (Fig. 1B). Crowns of three pairs of myosin heads emerge every 14.3 nm so that the headed half-thick filament, 700 nm long, carries (700/14.3·6=) 294 myosin motors.

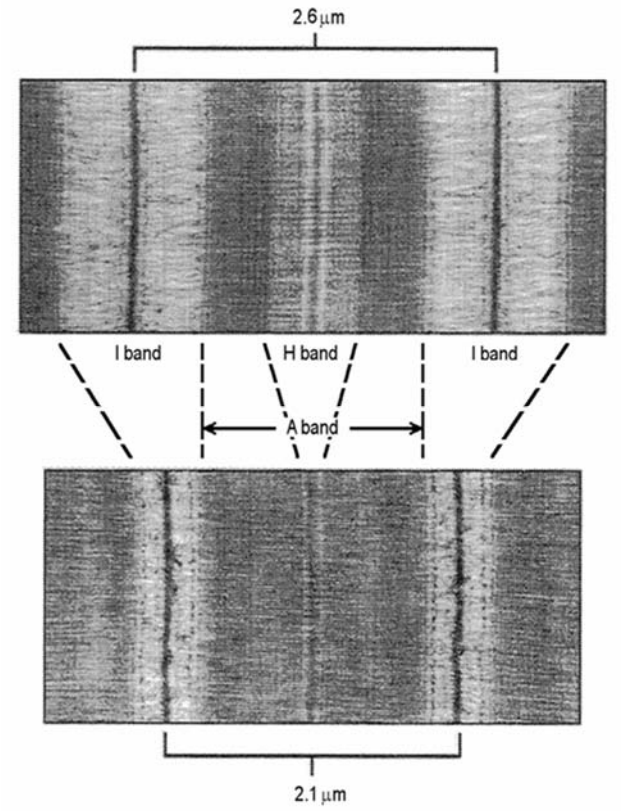

Figure 2. Electron micrograph images at two different sarcomere lengths. The increase from 2.1 to 2.6 μm implies change in the extent of overlap between actin e myosin filaments and thus in the width of the I and H bands.

The actin filament (F-actin) is generated by the polimerization of G-actin monomers, a globular protein of 5.5 nm in diameter and 42 kDa molecular weight, in a double stranded helix so that the axial repeat of monomers along the actin filament is 2.75 nm.

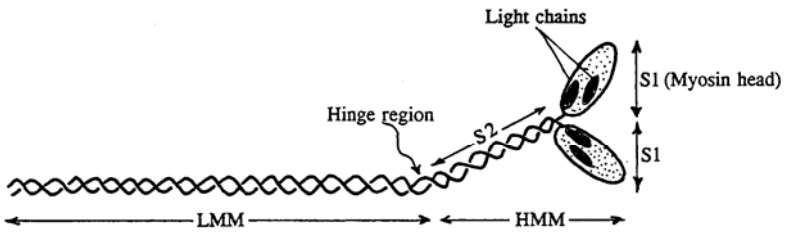

Figure 3. The myosin protein is made of two heavy chains and two pairs of light chains. Proteolytic digestion splits the heavy chain in a globular portion (S1) and a tail (S2 and LMM). The S2 portions and the LMMs have a coiled-coil structure.

1.1.2 Regulatory proteins

The activation of the thin filament is controlled by the regulatory proteins, the tropomyosin and the troponin complex (Fig. 1B). Tropomyosin polymerizes to form a filament lying in the groove between the two actin strands. The troponin complex, that repeats every seven actin monomers for the entire length of the filament, consists of three subunits, troponin I, troponin C that binds Ca^{2+}, and troponin T that binds to tropomyosin. When the myoplasmic calcium concentration increases, the calcium-sensitive troponin C triggers a series of structural changes that end with the movement of tropomyosin within the groove removing the steric inhibition of actin-myosin interaction. Myosin attachment to actin has been suggested to promote further movement of tropomyosin, allowing the full exposure of myosin binding sites on the actin filament.

1.1.3 Cytoskeletal proteins

The cytoskeletal proteins accomplish the mechanical role of maintaining the cell architecture, preventing damages to the membrane and transmitting the force outside. At the level of the Z line the protein α-actinin is the main component of the filamentous structure, which forms the tetragonal reticulum that allows each thin filament of a sarcomere to be connected to four thin filaments in the next sarcomere. Titin (Fig. 1B and C), a filamentous protein with a molecular weight of 3 MDa, diameter about 4 nm and length 1 μm, forms a filament running from the Z line to the M line making contact with both myosin and actin filaments. Titin represents a scaffold for the thick filament assembly and constitutes an elastic element, in parallel with myosin motors, accounting for the passive force of the fibre at long sarcomere lengths. The dynamic interaction of titin with the actin filament suggests also a possible regulatory action of acto-myosin activity.

Nebulin (800 kDa molecular weight) forms an inextensible filament, running from the Z line to the end of the thin filament (Fig. 1B and C), where it binds to tropomodulin, the thin filament pointed-end capping protein. Nebulin has an important role in modulating acto-myosin interaction (Bang *et al.*, 2009). Another sarcomeric protein is the Myosin Binding Protein C, MyBP-C that is confined to the "C-zone" of the thick filament, from 250 nm to 510 nm from the filament midpoint in Amphibia, and is able to form bridges from the thick to the thin filament at rest (Luther *et al.*, 2011).

1.2 The tilting lever arm model of the myosin working stroke

The description of the crystallographic structures of both actin (Kabsch *et al.*, 1990) and myosin (Rayment *et al.*, 1993b) molecules allowed to define a model for the structural working stroke in the motor domain responsible for the generation of force and shortening in muscle.

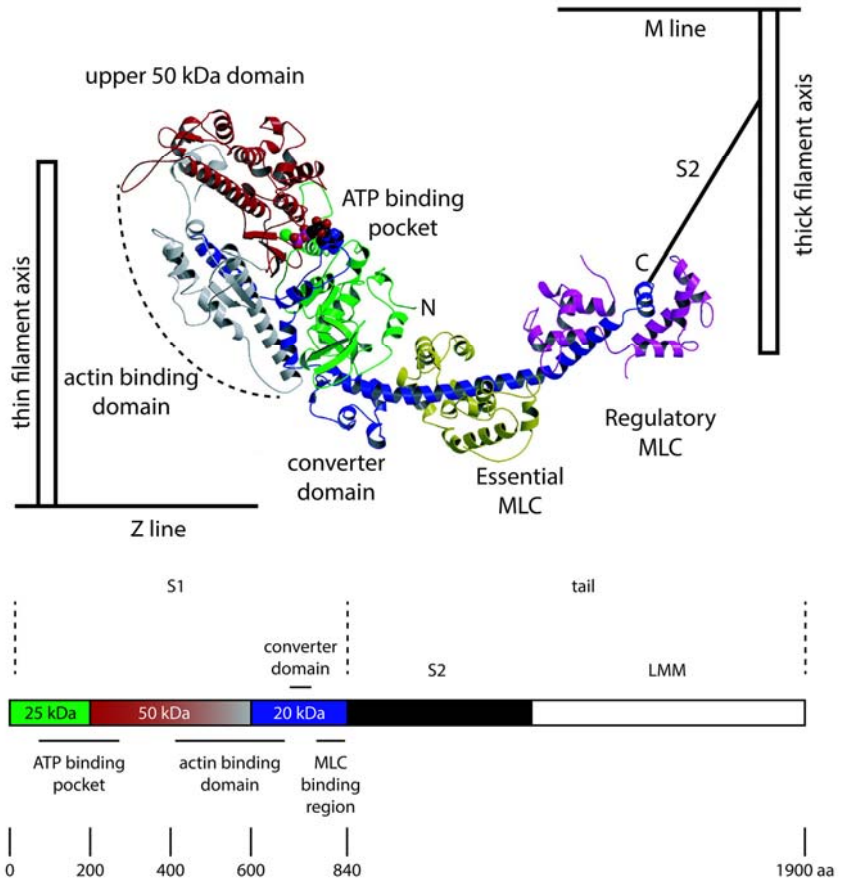

Figure 4. Upper panel: Ribbon representation of the S1 crystallographic structure (Rayment *et al.*, 1993b). The proteolytic fragments are colour coded: 25 kDa (N-terminal) green; 50 kDa red-grey; and 20 kDa (C-terminal) blue. The 50 kDa fragment spans two domains: the 50 kDa upper domain and the 50 kDa lower domain or actin binding domain. The actin binding site is grey. The C-terminal tail or "neck" carries two calmodulin-like light chains: the regulatory light chain (magenta) and the essential light chain (yellow). **Lower panel:** Schematic representation of the primary structure of complete MHC with indication of the functional relevant sequences.

The S1 portion, crystallised either without nucleotide or with different nucleotide analogues, allowed the definition of the structure of different biochemical states (Rayment *et al.*, 1993b). The first structure to be resolved was the nucleotide-free state of S1 from chicken skeletal muscle. S1 is made of three segments, previously identified by proteolysis (Fig. 4): the amino-terminal segment (25 kDa domain, green), the motor domain (MD) or catalytic domain (CD) (red, upper 50 kDa domain and light grey, lower 50 kDa domain), that has both the actin binding site and the ATP binding site, and the light chain binding domain (LCD) (20 kDa, blue), constituted by an α-helix that connects the carboxyl-terminal of the head to the S2 α-helix (the rod). Two light chains, the essential light chain (ELC, yellow) and the regulatory light chain (RLC, magenta), are associated to the 20 kDa domain. Between the CD and the LCD there is a small compact domain called the converter domain (Holmes, 1997; Dominguez *et al.*, 1998). Because of the absence of ATP, this structure was associated to the rigor state, attained by the muscle after death. This structure of the myosin is assumed to be that at the end of the working stroke (Dobbie *et al.*, 1998).

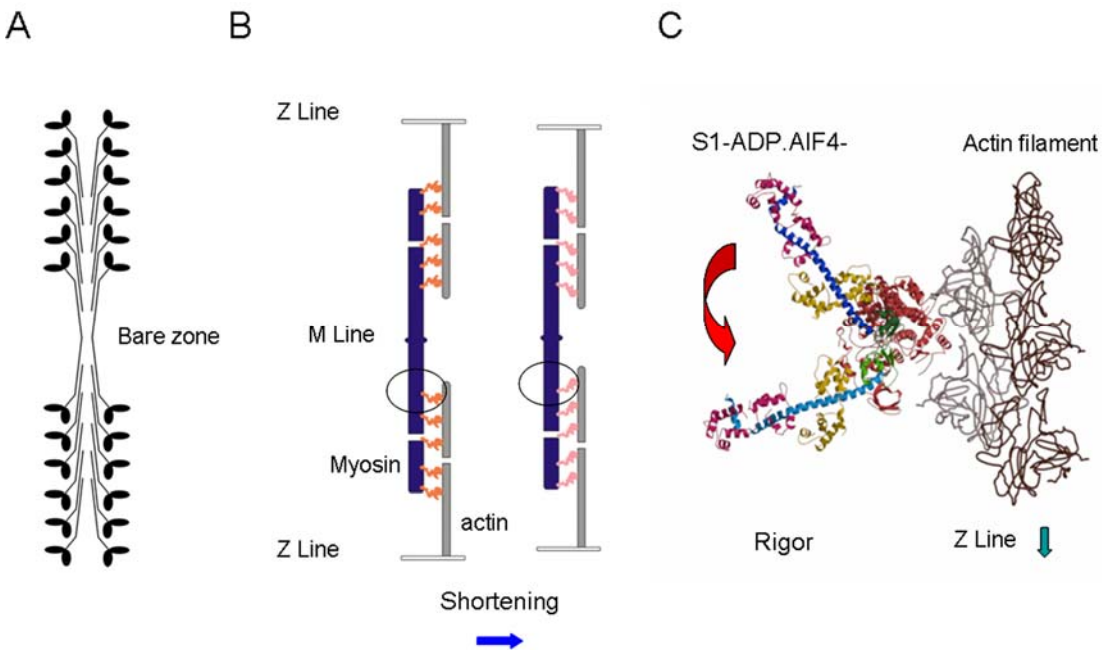

Figure 5. **A.** Arrangement of the myosin molecules in the thick filament. **B.** Schematic diagram of the sarcomere with the two arrays of myosin heads (red) protruding from the thick filament (blue) attached to the actin filament (grey) at the beginning of the working stroke (like during the isometric contraction, left panel) and at the end of the working stroke (like following shortening, right panel). In circles are the myosin heads conformations like in C. **C.** Crystallographic structure of rigor-S1 (LCD light blue) and (ADP)AlF^-_4 (LCD dark blue). CD (red), RLC (magenta), ELC (yellow), converter region (light and dark green), actin monomers (brown and grey).

A model for the state at the beginning of the working stroke has been obtained by using non hydrolysable analogues of the ATP, like Mg.ADP.AlF^-_4 and Mg.ADP.BeFx (Fisher *et al.*, 1995; Dominguez *et al.*, 1998). The superposition of the structural model of the acto-myosin complex in

the two states, based on the low resolution electron density maps of the actin filaments decorated with myosin, shows that the working stroke consists in a 70° change in the orientation of the LCD relative to the CD, firmly attached to actin, as a consequence of a structural change in the converter domain (Fig. 5). The LCD acts as a lever arm that amplifies the movement at the level of the head-rod junction (tilting lever arm model), where the 70° rotation of the LCD corresponds to an axial movement of ~ 10 nm.

1.3 The coupling between biochemical and mechanical steps of the actin-myosin interaction

Solution studies of the actin-myosin reaction (Lymn & Taylor, 1971) showed that myosin (M) is an actin activated ATPase which uses MgATP as a substrate. The myosin ATPase pathway in the presence of actin is shown in Scheme 1. In the absence of nucleotide the motor binds tightly to the actin (AM, rigor state). The binding of ATP dissociates the actomyosin complex (M.ATP + A), then ATP is hydrolysed to inorganic phosphate (Pi) and ADP that remain in the catalytic site of S1. Myosin with the hydrolysis products has a high affinity for actin and in the presence of actin binds to it (AM.ADP.Pi). In this state the affinity of myosin for the hydrolysis products reduces; Pi is released first, with a large enthalpy change, then ADP is released. Release of ADP allows a new ATP molecule to bind to myosin and the cycle starts again.

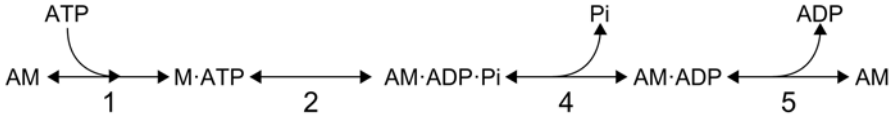

Scheme 1

The structural states of the myosin motor suggested by the crystallograhic studies (Fig. 5) are associated to the biochemical states of the Lymn and Taylor (1971) cycle, as summarized in Fig. 6 (Nyitrai & Geeves, 2004; Geeves & Holmes, 2005). The transition from (*a*) to (*b*) represents the working stroke and is associated to Pi release, the step that is accompanied by the largest enthalpy change in solution (White & Taylor, 1976). In the structured system this enthalpy change shows up as a working stroke dependent development of strain between the two filaments, which is shown in state (*b*) as the extension of an elastic element in the S2 portion connecting the motor domain to the thick filament. If the load opposing to the stroke is low, the strain is prevented by the movement of the lever arm toward the end of the working stroke (state (*c*)). ADP release can occur from either state (*b*), the strained A.M$^{\#}$.ADP state, or state (*c*), A.M.ADP, the state in which the strain is relieved because the load is low and the relative sliding of the two filaments is allowed.

Recent *in situ* experiments suggested that the working stroke and release of hydrolysis products are independent processes with the rate of Pi and ADP releases increasing with the progression through the working stroke (Caremani *et al.*, 2013, 2015).

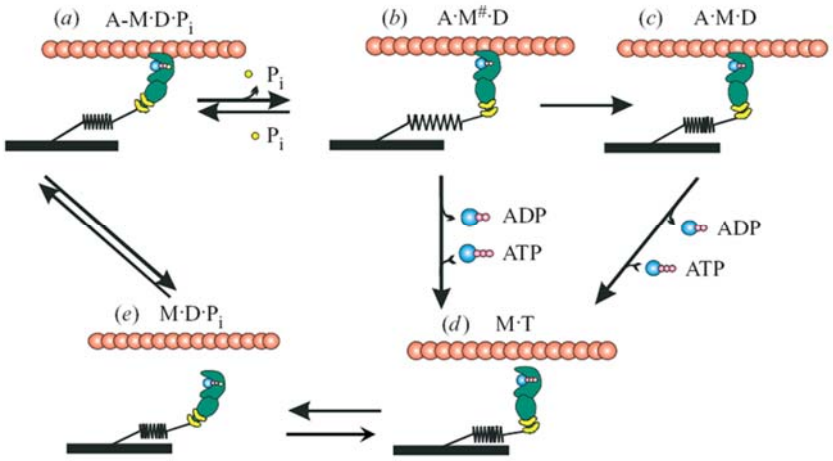

Figure 6. Chemo-mechanical cross-bridge cycle. The cross-bridge cycle is shown essentially as described by (Lymn & Taylor, 1971) but with a strain-dependent cross-bridge detachment step. (*a*)-(*e*) identify the different mechanical states in the structured system (cartoons, orange circles: individual actin sites, green: myosin motor domain, yellow: light chains, blue: adenosine attached to two or three phosphates in red or yellow after hydrolysis) and the corresponding biochemical states (A, actin, M, myosin; T, ATP; D, ADP).

The rates and the equilibrium constant of the cycle are affected by changes in amino acid sequence in the CD of the myosin. The whole cycle can proceed at very different overall velocities and with variation of the fraction of the ATPase cycle time the motor spends attached to actin (duty cycle) for different MHC isoforms (for a recent review, see (Walklate *et al.*, 2016)).

1.4 The kinetic and mechanical properties of the myosin motor

The minimal functional unit in muscle is the array of myosin motors overlapping with the actin filament in each half-sarcomere. The properties of this collective motor can be understood only preserving the supramolecular organization represented by the half-sarcomere. Single fibres from frog skeletal muscle have been the most suitable preparation for investigation on the functional unit, because they can be isolated intact and studied with mechanical control at the level of a selected population of sarcomeres (Huxley & Simmons, 1971; Lombardi & Piazzesi, 1990). Under these conditions the action of the motors can be synchronized with step perturbations in length or load, and their mechanical and kinetic properties can be investigated.

1.4.1 Isometric force transients

The response of an actively contracting fibre to a stepwise change in sarcomere length of a few nanometers is a force transient made of four phases (Fig. 7). Phase 1, the change in force simultaneous with the step, is due to the elastic properties of the half-sarcomere components, myofilaments and myosin motors; the extreme tension at the end of the step is called T_1 and is roughly proportional to the step size, as expected from a linear elasticity. Phase 2, the rapid force recovery complete in 1-2 ms, is the mechanical manifestation of the execution of the working stroke by the motors attached to actin. The force attained in phase 2 is named T_2. The following phases consist of a pause in the recovery of force, phase 3, followed by a slow return to the isometric plateau value (T_0), phase 4, due to detachment and reattachment of myosin motors.

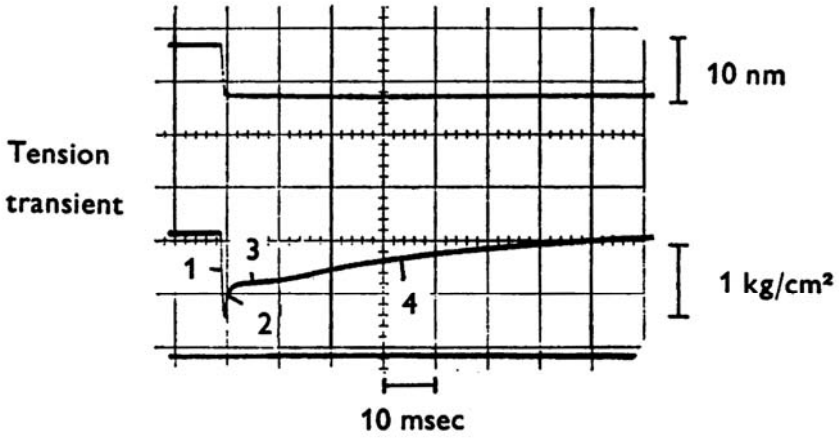

Figure 7. Force transient (lower trace) elicited when length is suddenly altered (upper trace). Bottom trace is force baseline. The numbers indicate corresponding phases as described in the text (from Fig. 7 (Huxley, 1974).

The first two phases of the force transient describe the properties of the myosin motors attached to actin (Huxley & Simmons, 1971; Ford *et al.*, 1977). The slope of the relation between T_1, the peak force attained with the step, and the step amplitude (T_1 relation, filled circles in Fig. 8A) estimates the stiffness of half-sarcomere elasticity and the intercept of the relation on the abscissa, Y_0, estimates the strain of this elasticity at the force (T_0) just before the step. The plot of the force T_2, attained at the end of the 1-2 ms force recovery following the step, versus the step amplitude (T_2 relation, open circles in Fig. 8A) points out the non-linearity of the quick recovery process: the tension recovery is almost complete for releases up to 5 nm per half-sarcomere, then decreases becoming zero for a release of about 11nm. The other non-linearity of this process concerns the rate at which force is recovered, that varies with the direction and the amplitude of the step, reducing from the largest releases to the largest stretches (Fig. 8B). These two non linearities exclude that the force recovery could be explained by passive viscoelasticity where a damped elastic element V_2 is in series with an

undamped elastic element V_1 (Voigt element, inset in Fig. 8A) and indicate that phase 2 recovery is due to the active properties of the myosin motor (Huxley & Simmons, 1971). Huxley and Simmons interpreted phase 2 recovery as due to strain dependent transition through different conformations (different force-generating states) of the motor. State transitions, occurring at a rate of 10^3 s^{-1}, allow the motor to maintain the isometric force for about 5 nm of shortening and (in agreement with the crystallographic model) produce a maximum shortening of 11 nm, as estimated by the abscissa intercept of the T_2 relation.

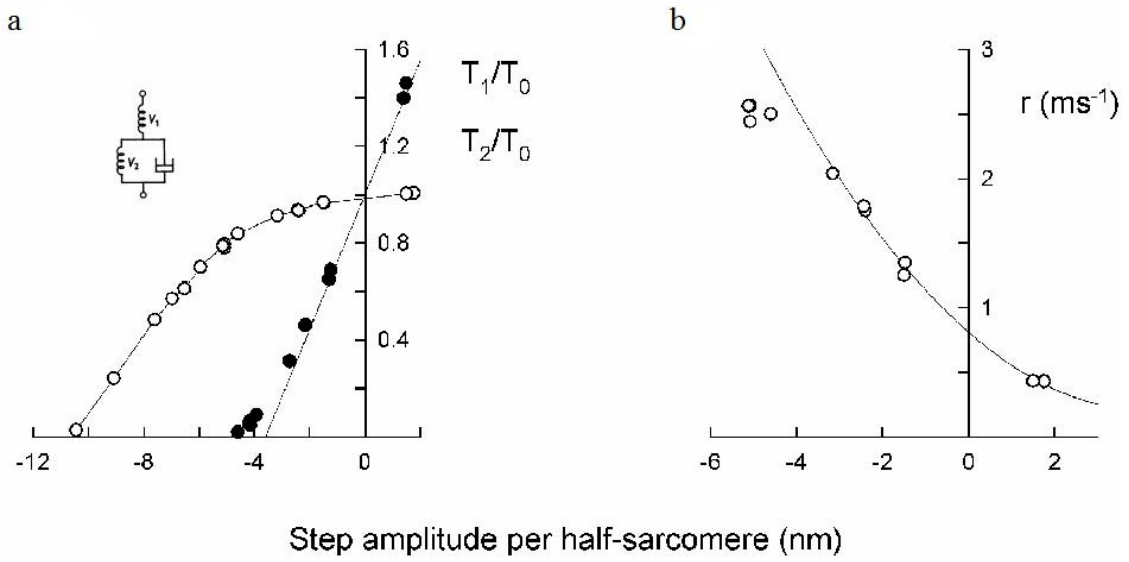

Figure 8. A. Relations between T_1 (filled circles) and T_2 (open circles) and step amplitude. The straight line is interpolated through experimental T_1 points for small steps. The abscissa intercept (Y_0) is 3.6 nm. T_2 points are joined by eye. The mechanical model in the inset is the *Voigt element*. **B.** Relation of rate of quick force recovery (r) and step amplitude. r is estimated by the reciprocal of the time necessary to attain 63% of the T_2 recovery. The solid line is obtained by fitting r data points with a parabola(adapted from, (Piazzesi & Lombardi, 1995).

There are evidences that the half-sarcomere compliance is constituted by myofilaments (actin and myosin) as well as by the attached myosin motors (Huxley *et al.*, 1994; Wakabayashi *et al.*, 1994). Myofilament compliance, being in series, makes the kinetics of force recovery following the step unable to correctly describe the kinetic state transition in the motors (Linari *et al.*, 2009). The contribution of the myofilament compliance to the response to a step can be eliminated by imposing the step in force clamp on an otherwise isometric contraction (Piazzesi *et al.*, 2002). In this case the elastic response is followed by a length transient that occurs under isotonic conditions and thus allows to obtain direct information on the kinetics of the working stroke without the influence of the length changes in the series compliance (Piazzesi *et al.*, 2002; Reconditi *et al.*, 2004; Piazzesi *et al.*, 2007; Piazzesi *et al.*, 2014).

1.4.2 Isotonic velocity transients

When a stepwise drop in force below the isometric value (T_0) is superimposed on an isometric contraction, the fibre undergoes a multiphase shortening response, the so called velocity transient, before attaining a steady shortening velocity, characteristic of the force-velocity (*T-V*) relation (Fig. 9A).

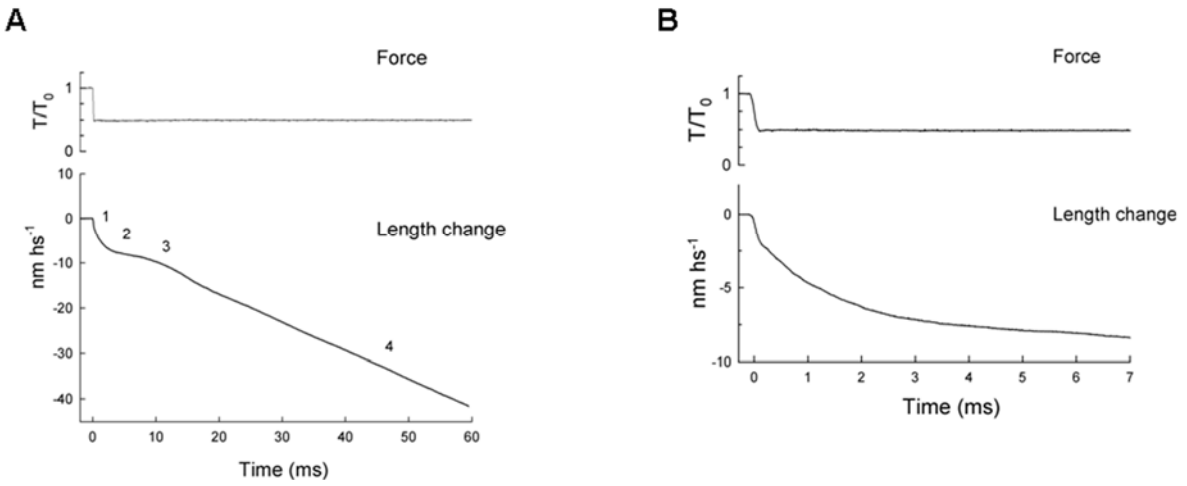

Figure 9. Isotonic velocity transient following a force step to 0.5 T_0 (adapted from (Piazzesi *et al.*, 2002). **A.** Force (upper trace) and hs length change (lower trace) on slow time scale showing all the phases of the velocity transient. **B.** Same length response as in A on a faster time scale, showing only early phases (1 and 2).

The shortening simultaneous with the force step (phase 1) is followed by a rapid shortening, lasting for a few milliseconds (phase 2); the velocity then decreases to a minimum value (phase 3), and then increases again to attain the steady state value (phase 4). Phase 1 is due to the elasticity of the half-sarcomere and phase 2 is the manifestation of the working stroke in the attached motors, synchronized by the drop in force. Both the size and the speed of the working stroke reduce with the increase in the load (Reconditi *et al.*, 2004). Phase 3 is due to motors detaching at the end of their stroke, followed by reattachment farther from the centre of the sarcomere. Phase 4 is the steady shortening accounted for by detachment/attachment rates in asynchronously cycling motors (Piazzesi *et al.*, 2007).

The velocity of steady shortening has a hyperbolic dependence on the load (force-velocity relation *T-V*, Fig. 10). Under unloaded conditions no force is produced and the fibre shortens at its maximum velocity, V_0. The velocity reduces increasing the load and becomes zero when the load corresponds to the force the fibre develops under isometric conditions (T_0).

The *T-V* relation is the same, whether the independent variable is the velocity of shortening or the force. In Fig. 10 the conventional representation is used, with the force on the abscissa and the velocity on the ordinate. The relation can be described by the Hill's hyperbolic relation (Hill, 1938):

$$(T+a)\cdot(V+b)=(T_0+a)\cdot b \qquad \text{eqn (1)}$$

where a and b are constants with the dimension of force and velocity, respectively. The intercept on the force axis is the isometric force T_0, while the intercept on the velocity axis is the maximum shortening velocity, V_0, that is the velocity of unloaded shortening.

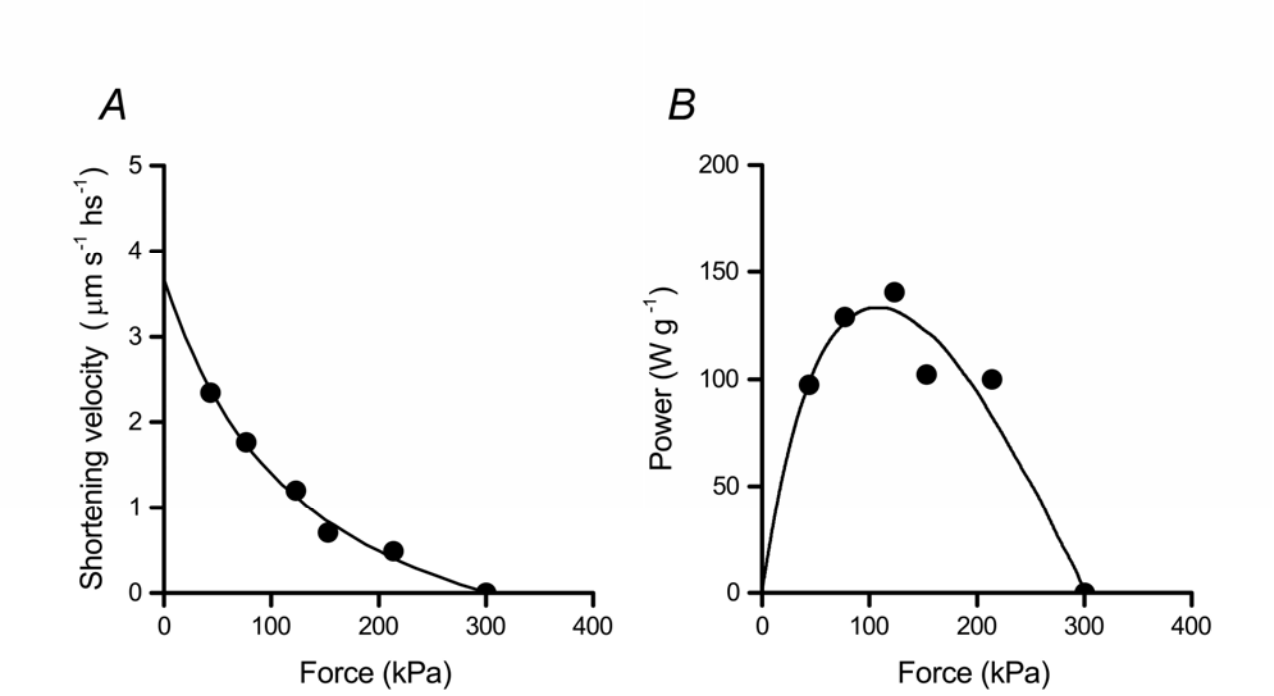

Figure 10 Force-velocity (A) and force-power (B) relation from a single muscle fibre at 4° C (*Rana temporaria*, tibialis anterior muscle). Power is obtained by the product between force and velocity. Line in A is the hyperbolic Hill's equation fit to the data.

For comparison among different muscle types, it is convenient to write Hill's equation in a form in which all terms are dimensionless, that is, with force and velocity expressed in relative units T/T_0 and V/V_0, respectively:

$$(T/T_0+a/T_0)\cdot(V/V_0+b/V_0)=(1+a/T_0)\cdot b/V_0 \qquad \text{eqn (2)}$$

The term a/T_0 is a measure of the curvature of the force-velocity relation, a parameter that is related to the maximum mechanical power $W(=T\cdot V)$. In fact the lower the curvature the larger the product $T\cdot V$ at intermediate loads, when the power is maximum.

1.5 Mechanical properties of myofilaments and myosin motors

If the elasticity responsible for phase 1 of the transients were fully accounted for by the motors and the myofilaments were infinitely stiff, the half-sarcomere stiffness would be a direct measure of the fraction of motors attached to actin. However, there is evidence that almost ½ of the half-sarcomere compliance resides in the myofilaments (Huxley *et al.*, 1994; Wakabayashi *et al.*, 1994; Dobbie *et al.*, 1998; Linari *et al.*, 1998; Reconditi *et al.*, 2004). The compliance of myofilaments and myosin motors is distributed along each half-sarcomere in a complex network of series-parallel springs; however it is possible to reduce the system to a simple mechanical model with three main compliances in series (actin and myosin filament and motor compliances) so that an equivalent filament compliance (C_f) can be calculated as the sum of the equivalent compliances of the actin and myosin filaments (Ford *et al.*, 1981) (Fig. 11, Model 1).

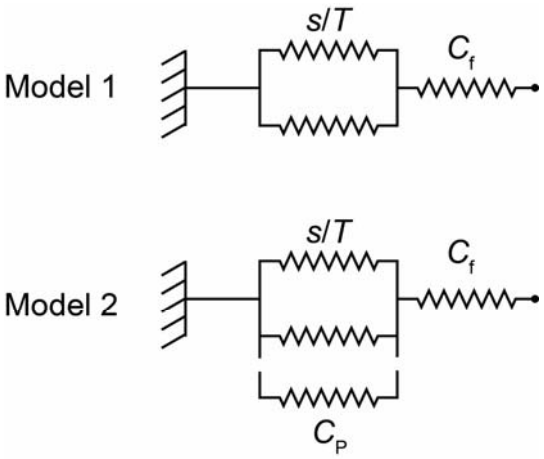

Figure 11. Models representing the elements contributing to the half-sarcomere compliance. In Model 1, the myofilament compliance (C_f) is in series with an array of myosin motor (only three are shown) with a constant strain (s). The isometric force (T_0) increases with the increase in number of attached motors. In Model 2 an elastic element with compliance C_P (grey) is in parallel with the array of motors. As previously described (Fusi *et al.*, 2014), the model can be used to determine the contribute of the various elements to the half-sarcomere compliance.

The half-sarcomere compliance (C_{hs}) is thus given by: $C_{hs}=C_f+s/T$ where C_f is the equivalent filament compliance, and s/T (where s is the average strain in the attached motors and T is the force) is the motor compliance. In conditions in which T increases only for the increase in number of motors, s remains constant and the compliance of the motor array changes in an inverse proportion with T. In fact, it has been found in both intact fibres from frog tibialis anterior muscle (Fusi et al. 2014 and references therein) and skinned fibres from rabbit psoas muscle (Martyn *et al.*, 2002; Linari *et al.*, 2007; Seebohm *et al.*, 2009) that the half-sarcomere strain (Y) increases with T in proportion to the increase in filament strain according to Model 1 in Fig. 11, where Y is given by:

$$Y(T) = C_f \cdot T + s \qquad \text{eqn (3)}$$

During force development in an isometric tetanus of intact fibres, eqn (3) can be applied in the range of forces > 40 kPa to estimate C_f and s from the slope and the ordinate intercept, respectively, of the half-sarcomere strain-force relation (Linari *et al.*, 2009; Brunello *et al.*, 2014; Fusi *et al.*, 2014) (Fig. 12A). For forces < 40 kPa the relation shows a downward concavity indicating that the half-sarcomere compliance increases with the reduction of force by an amount that is less than that expected from the reduction of the number of myosin motors (Fig. 12B). This reveals the presence of an elastic element (C_P) with constant stiffness in parallel with the force generating motors (Model 2 in Fig. 11, see also; (Colombini *et al.*, 2010; Fusi *et al.*, 2014). This deviation is not evident in skinned fibres where the lattice spacing increases following skinning (Martyn *et al.*, 2002; Linari *et al.*, 2007; Seebohm *et al.*, 2009). According to Model 2 the half-sarcomere compliance (C_{hs}) is given by:

$$C_{hs}(T) = C_f + s \cdot C_P/(s + C_P \cdot T) \qquad \text{eqn (4)}$$

where C_P is the compliance of the elastic element in parallel with the force generating motors. In intact fibre, eqn (4) applied to the whole range of forces allow to estimate s, C_f and C_P (Fig. 12B). It must be noted that C_P is about 20 times larger than the compliance of the motor array at T_0 and thus it does not affect significantly the estimate of s with Model 1 (about 1.7 nm in both cases).

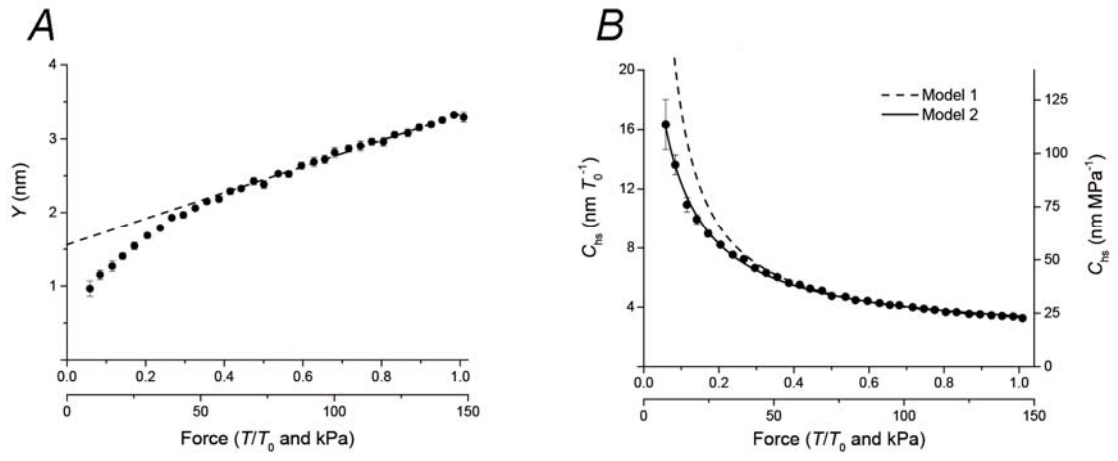

Figure 12 Mechanical parameters of the half-sarcomere during force development in isometric contraction. A, relation between hs strain (Y) and force. B, Half-sarcomere compliance (C_{hs}) fit with model 2 (continuous line). Dashed line is the relation predicted by model 1. Adapted from Figure 3, (Fusi *et al.*, 2014).

A correct estimate of myofilament compliance is a prerequisite for extracting the compliance of the motor array (s/T) and thus the number of attached motors from half-sarcomere stiffness

measurements. In turn, knowing the number of motors working in the half-sarcomere is fundamental for relating the mechanical properties of the half-sarcomere to those of the motors.

A direct estimate of myofilament compliance has been obtained with X-ray diffraction measurements of the changes with force of spacing of actin- and myosin-based reflections. These experiments provide a value of 0.23 % per T_0 (T_0 = 240 kPa, *Rana temporaria*, 4°C) for the compliance of the myosin filament (Reconditi *et al.*, 2004; Huxley *et al.*, 2006), corresponding to an equivalent compliance of 6.4 nm/MPa. The equivalent compliance of actin filament estimated with X-ray diffraction is 6.9 nm/MPa (Huxley *et al.*, 1994; Wakabayashi *et al.*, 1994; Dobbie *et al.*, 1998). Thus the equivalent filament compliance is (6.4 nm/MPa + 6.9 nm/MPa=) 13.3 nm/MPa. The total half-sarcomere compliance is obtained from the strain at T_0, Y_0 (4.9 nm from the above experiments with T_0 = 240 kPa) and is (4.9 nm / 0.24 MPa =) 20.4 nm/MPa. Hence the filament compliance in single fibres from *Rana temporaria* at 4 °C is 65% of the total half-sarcomere compliance at the isometric tetanus plateau, and the compliance of the array of motors is 35%. Similar values of filament compliance have been found for single fast fibres from dogfish (Park-Holohan *et al.*, 2012) and rabbit (Linari *et al.*, 2007).

Thus, in frog muscle, the compliance of the motor array at the plateau of an isometric contraction is (20.4 nm/MPa · 0.35 =) 7.14 nm/MPa, that is (7.14 nm/MPa · 0.24 MPa=) 1.71 nm/T_0 (Decostre *et al.*, 2005; Piazzesi *et al.*, 2007). The motor compliance becomes 0.5 nm/T_0 in rigor, when all the myosin heads are attached to actin (Piazzesi *et al.*, 2007). Since the motor compliance is inversely proportional to the number of attached motors, the ratio between the motor compliance in rigor and that in isometric contraction gives the fraction of motors in the half-sarcomere responsible for the isometric force, that is (0.5 nm/T_0 / 1.7 nm/T_0 =) 0.3 (Piazzesi *et al.*, 2007). Knowing this parameter, the isometric force per cross-sectional area, the density of myosin filaments in the cell of striated muscle and the number of heads per thick filament, it is possible to calculate the isometric force per attached motor and the related energetic parameters. From the isometric force per cross sectional area and the density of myosin heads in the half-sarcomere of the striated muscle of the frog (294 · $0.51 \cdot 10^{15} = 15 \cdot 10^{16}$ per m^2) (Barclay *et al.*, 2010a), the force per myosin head, results to be about 1.57 pN. If the fraction of myosin heads attached and generating force is 0.3, the average force per motor is (1.57 pN/0.3 =) 5.29 pN. With an average strain of 1.71 nm, the motor stiffness is about (5.29 pN/1.71 nm =) 3.09 pN/nm. A quite important conclusion from this bulk of mechanical data was that the motor stiffness is much larger than previously thought. In terms of Huxley and Simmons model for force generation (Huxley & Simmons, 1971) this implies that the conformation of the motors during isometric contraction is biased to the beginning of the working stroke and further progression in the stroke occurs only in contraction at lower loads.

1.6 Structural and functional differences between slow and fast muscle

Until the end of the 1960's the common view of the diversity in skeletal muscle was based on the classification of fast-twitch muscles (also called white muscles, with glycolytic metabolism and specialised for phasic activities) and slow muscles (also called red muscles, rich of myoglobin and oxidative enzymes and specialised for more continuous activity) (Needham, 1926) . The mechanical and biochemical aspects found their matching point in the correlation between the actin-activated ATPase activity of myosin and the speed of shortening (Barany, 1967).

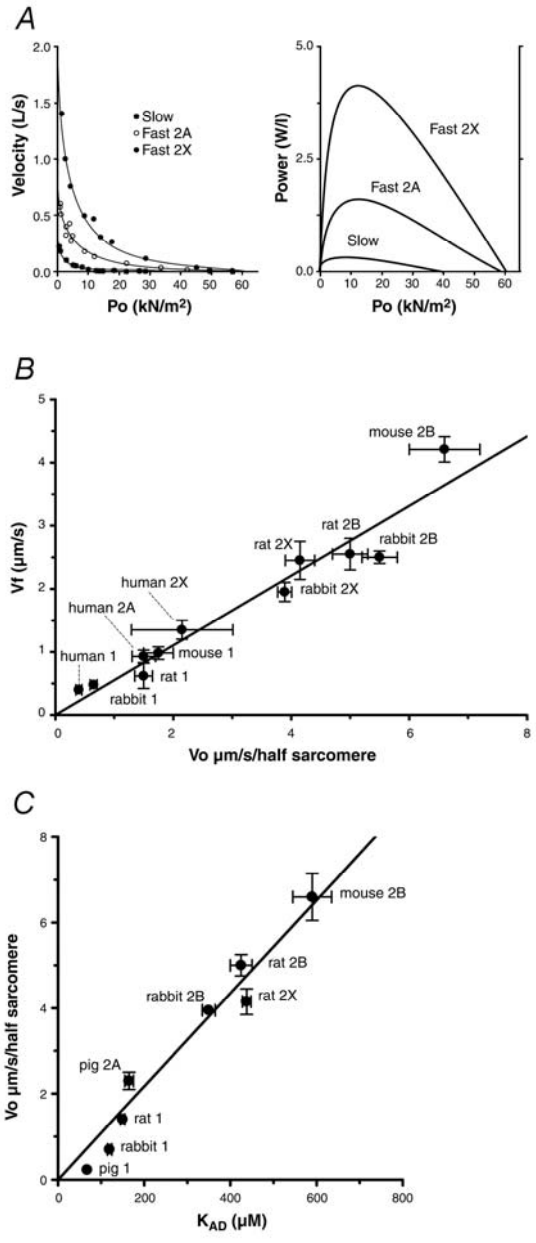

Figure 13. Mechanical and kinetic properties of slow and fast fibres. **A**: force-velocity (left panel) and force-power (right panel) relations of three skinned fibres from human (slow, fast 2A, and fast 2X) maximally activated at 12°C. **B**: correlation between sliding filament velocity of purified myosins (V_f) determined by in vitro motility assay at 25°C and unloaded shortening velocity of single skinned fibres (V_0) maximally activated at 12°C. Fibres were obtained from four different species (from (Pellegrino *et al.*, 2003)), correlation between V_0 and V_f and V_0 and ADP affinity (K_{AD}) was done for corresponding myosin isoforms from different muscles and different species (Nyitrai *et al.*, 2006). Modified from (Schiaffino & Reggiani, 2011).

Application of electron microscopy and biochemical techniques to slow and fast muscles allowed more information about them to be obtained. Fast twitch EDL muscle showed both small mitochondrial-rich and large mitochondria-poor muscle fibres, well developed sarcoplasmic reticulum (SR) and, in fibre containing fewer mitochondria, thin Z-line. In contrast slow-twitch soleus muscle showed small mitochondrial-rich, poorly developed SR and thick Z-line fibres. On these bases it was proposed that muscle fibre structure is an expression of two different mechanical parameters: speed of contraction, related with development of SR, and resistance to fatigue, correlated with mitochondria content and thickness of the Z-line (Schiaffino *et al.*, 1970). Development of histochemical methods for myosin ATPase allowed to distinguish type 1 fibres, predominant in the slow-twitch muscle from two fibre populations, type 2A and 2B fibres, abundant in fast-twitch muscle (Guth & Samaha, 1969). In the 1990's, the use of monoclonal antibodies against MHC led to the identification of fibres called 2X or 2D (Schiaffino *et al.*, 1989; LaFramboise *et al.*, 1990). The mechanical performance of muscle fibres expressing different MHC isoforms has been characterised in terms of power and efficiency in mammalian skinned fibres (10-20°C). Comparison of muscle fibres that express either slow or one of the fast myosin (2A, 2X and 2B), showed that peak power increases progressively from slow to fast 2A, fast 2X and fast 2B fibres (Fig. 13A), which exhibit the highest values in all mammalian species and all muscles examined up to now (Bottinelli *et al.*, 1991; Bottinelli *et al.*, 1996; Gilliver *et al.*, 2009), with a range of maximum power up to 10-fold that of slow muscle. V_0, as determined by the force-velocity relation (see Fig. 10A) and the filament sliding velocity (V_f) in *in-vitro* motility assay (IVMA), showed that the myosin isoforms determine the speed at which actin filament can slide under the action of myosin motors. In fact, there is a strong correlation between V_f and V_0 determined on purified myosin isoforms and in muscle fibres containing the same myosin isoform (Fig. 13 B) (Pellegrino *et al.*, 2003). In terms of kinetics of the acto-myosin ATPase cycle the rate of ADP dissociation may limit V_0 in both slow and fast fibres (Fig. 13C) (Nyitrai *et al.*, 2006; Schiaffino & Reggiani, 2011). Measurements of steady state ATPase activity in skinned fibres have shown that ATP hydrolysis rate increases from fibres expressing slow myosin to fibres expressing fast 2A, 2X and 2B fibres (Potma & Stienen, 1995; He *et al.*, 2000; Han *et al.*, 2003). The ratio between power and ATPase rate at different load gives the thermodynamic efficiency, the maximum value of which in slow fibres is similar to (Barclay *et al.*, 1993; He *et al.*, 2000) or higher than (Woledge, 1968; Barclay *et al.*, 2010b) that in fast fibres.

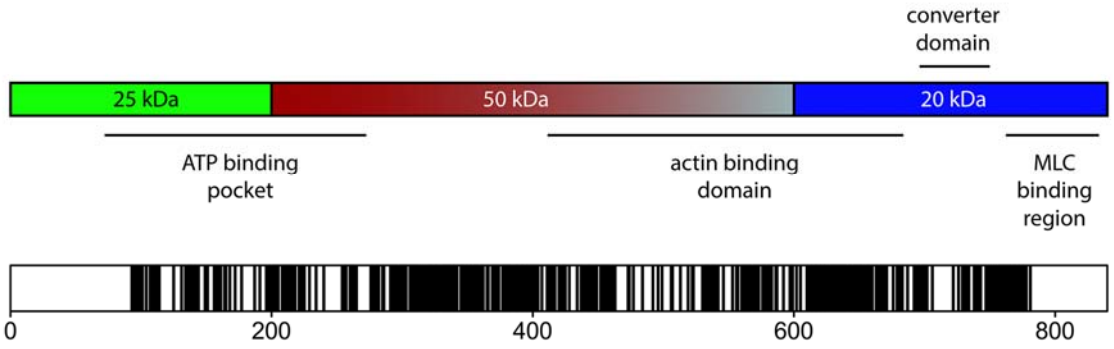

Figure 14. Localizations of the regions where diversity between isoforms tend to cluster (black bands) in paired comparison between the S1 portion of MHC-1 and MHC-2X of rabbit. Amino acid sequences (89-769) from NCBI protein database are aligned with Clustalw 2.1

How are these functional differences related to the primary structure of MHC? Comparison of the amino acid sequence in the S1 portion of the MHC of slow and fast (2X) isoforms (Fig. 14) shows that there are regions where diversity between isoforms tends to cluster.

In slow fibres from soleus muscle of human it has been found that a single natural occurring mutation in the converter domain (708-780 region) of the slow β-MHC isoform is responsible for a large change in motor stiffness. In fact, when arginine (R) in position 719 or in position 723 is replaced with tryptophane (W)(R719W) or glycine (G)(R723G) respectively, the stiffness of the myosin motor increases by 2-3 times (Kohler *et al.*, 2002; Seebohm *et al.*, 2009; Brenner *et al.*, 2014). Comparison of the available amino acid sequence of the converter domain between the slow and fast MHC isoforms of six species of mammals of different size (mouse, cattle, rabbit, pig, dog and human, Fig. 15) shows a difference in the amino acid content of about 55% in rabbit, much larger than that found in the other species (16-20% difference).

Figure 15. Amino acid sequences of the converter domain of MHC-1 and MHC-2X isoforms in six species of mammals. Numbers at the beginning and at the end of each sequence are the residues of start and end of the domain. Differences between slow and fast isoforms within a species are in bold. While the sequence of MHC-2X is similar among species, the sequence of MHC-1 is not.

The larger difference is related to the amino acid composition of the converter domain of the slow MHC isoform in rabbit with respect to the slow MHC isoform of the other species while the converter domain of the fast MHC isoform is well preserved among species. If the converter domain plays a major role in determining the motor stiffness, not only there should be a difference in stiffness between fast and slow isoforms, but also the different species should exhibit a relatively constant stiffness of the fast myosin isoforms and a larger variability in the stiffness of the slow isoforms.

Aims

The work described in this thesis is aimed at investigating *in situ* the mechanical and kinetic bases of the functional diversity of the isoform of the myosin motor present in slow skeletal muscles in terms of both the properties of the single motor and of the motor ensemble in the half-sarcomere. For this the mechanical parameters of the myosin motor (force, stiffness and size and speed of the working stroke) and of the motor ensemble (number of motors attached to actin, kinetics of the attachment-detachment) have been determined in demembranated fibres from a slow skeletal muscle of the rabbit, the soleus, and compared to those from a fast muscle, the psoas. Apart the ten times slower kinetics of both the working stroke and the motor attachment-detachment, the most relevant result is that the slow myosin isoform has a stiffness three times smaller than the fast isoform. This finding suggests that the stiffness of the myosin motor is a determinant of the isoform-dependent functional diversity between skeletal muscles and opens the question on the molecular mechanism for the high efficiency of the slow muscle.

Chapter 2 - Methods

2.1 Muscle fibre preparation

Experiments were done on chemically skinned fibre segments obtained from psoas and soleus muscles of adult male New Zealand white rabbit (weight 3-5 kg). Rabbits were killed by injection of an overdose of sodium pentobarbital (150 mg/Kg) in the marginal ear vein, in accordance with the Italian regulation on animal experimentation (Authorization 956/2015-PR in compliance with Decreto Legislativo 26/2014). The study was approved by the Ethical Committee for Animal Experiments of the University of Florence. Three rabbits were used for this work. Small bundles of 70-150 fibres from soleus and psoas muscles were stored in skinning solution containing 50% glycerol (storage solution, Table 1) at -20 °C for 3-4 weeks. Just before the experiment a bundle of fibres was transferred to a Petri dish kept at 4-6°C and with the bottom covered by a layer of Sylgard (Sylgard 184, Down Corning). Single fibres were then dissected under stereomicroscope (Stemi SV11, Zeiss) with dark field illumination and pinned down on the Sylgard surface at both ends. Fibres were treated with relaxing solution (Table 1) containing Triton X-100 (1% v/v) for 1-2 minutes at about 1 °C to ensure the complete removal of internal membranes. A fragment of fibre, 5-6 mm long, was cut and aluminium T-clips were mounted at its extremities for attachment to transducer hooks. In all the experimental solutions (see Table 1) the increase of interfilamentary spacing following permeabilization was reversed by osmotic compression with the osmotic agent Dextran T-500 (Pharmacia Biotech) (Brenner & Yu, 1991; Kawai *et al.*, 1993; Linari *et al.*, 2007). Based on the finding that resting intact slow and fast muscle fibres from mice have about the same interfilamentary distance (Zappe & Maeda, 1985) and assuming that the same amount of swelling occurs following skinning in slow as in fast rabbit muscle fibres, we added the same amount of dextran to the solution bathing both fibre types (4g/100ml or 4%) (Matsubara & Elliott, 1972; Maughan & Godt, 1979; Brenner & Yu, 1991; Kawai *et al.*, 1993; Linari *et al.*, 1998; Linari *et al.*, 2007).

2.2 Experimental set-up

The fibre was mounted in a drop of relaxing solution between the lever arms of a loudspeaker motor and a force transducer. A rapid solution exchange system, driven by a stepper motor, allows

rapid change of the solution bathing the fibre; a striation follower continuously records the length changes of a selected population of sarcomeres (Fig. 16).

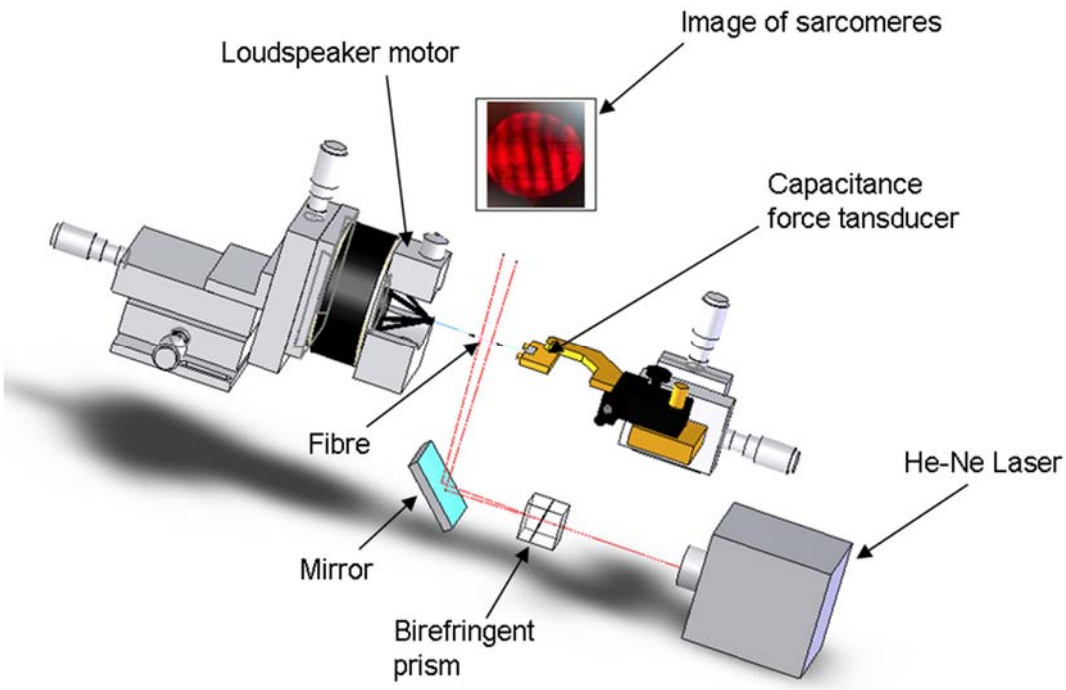

Figure 16. Schematic drawing of the experimental mechanical set-up. Muscle fibre is mounted between the levers of a loudspeaker motor (left) and a capacitance force transducer (right). Half-sarcomere length is monitored by means of a striation follower. A He-Ne laser beam is split by the birefringent prism into two beams focused on the fibre. The diffraction beams are collected by the optics of the striation follower giving an image of the sarcomeres as a sinusoidal intensity distribution of light.

2.2.1 Loudspeaker motor

A loudspeaker coil motor similar to that previously described (Lombardi & Piazzesi, 1990) was used to impose length changes on the fibre (Fig. 17). The system is made of a source of light, two photodiodes and a modified loudspeaker, where the cone is substituted with a pyramidal structure in carbon fibre directly stuck to the coil. A stainless steel lever (300 µm diameter) is glued on the top of the pyramid at one extremity, whereas it has a hook at its distal end. The lamp and the photodiodes are mounted on two aluminium plates, placed one in front of the other

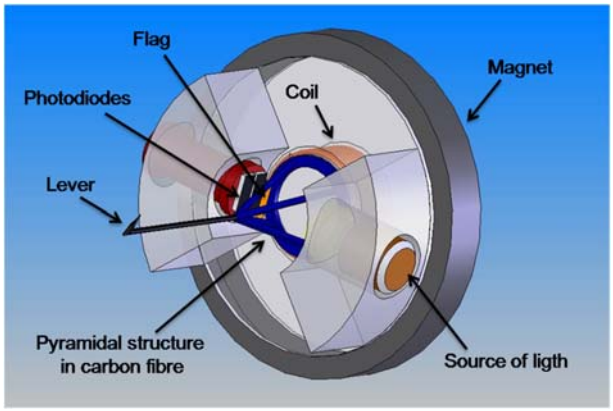

Figure 17. Diagram of the loudspeaker motor

on the loudspeaker iron plate. A flag, glued between two of the pyramid pillars in front of the photodiodes, partially cuts off the light beam directed to the photodiodes so that the movement of the coil and of the pyramid produces proportional changes in their illumination. The two photodiodes are differentially connected in order to double the sensitivity and remove the effects of diffused light. The position of the motor lever is servo-controlled by a feed-back circuit in which the feed-back signal is the output of the photodiodes (fixed-end mode), or the output of the force transducer (load-clamp mode). In fixed-end mode the output of the photodiodes is compared with the control signal which can be either zero (isometric conditions) or a step or/and ramp that change the position of the lever and thus the length of the fibre. In the load clamp experiments the motor is first operated in fixed-end mode and then, at the isometric force (T_0), is switched to load-clamp mode and the force is brought to a value that is a fraction of T_0. The maximal extent of the linear displacement of the motor is ± 300 μm.

2.2.2 Capacitance force transducer

The force developed by the fibre was measured by means of a capacitance force transducer similar to that described by (Huxley & Lombardi, 1980). The transducer is composed of two fused quartz plates (one fixed and one mobile), metallized with gold deposition on the facing sides that form a capacitor. Part of the metallization on the fixed plate is removed so as to isolate the central area used as the live electrode. The mobile plate is kept at 6-10 μm from the fixed one by interposition of gold foils (Fig. 18), which also provide electrical connection to the metallization on the moving plate. The force produced by the muscle fibre is directly applied to the centre of the moving plate by means of a glass lever hook (5-7 mm of length, 100-125 μm of diameter), attached to it. The bending of the moving plate, caused by the applied force, changes the air gap between the conducting surfaces of the two plates and thus the capacitance of the transducer. Capacitance changes are detected with a phase-discriminator circuit (Cambridge & Haines, 1959; Cecchi, 1983). With this circuit the sensitivity of the force transducers ranges from 80 to 250 V/N and the noise from 2 to 10 mV peak to peak (Huxley & Lombardi, 1980). The resonance frequency of the force transducer used here ranged from 30 to 50 kHz. In load clamp

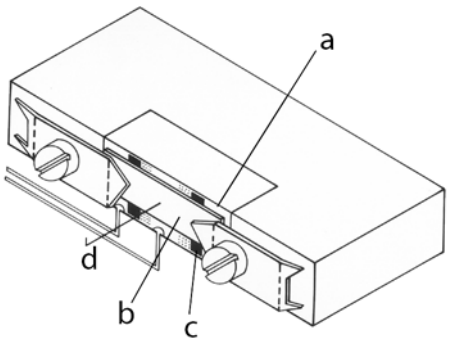

Figure 17. Diagram of capacitance force transducer; a, fixed plate; b, moving plate with attached glass lever hook; c, gold foils; d, glass lever hook.

experiments, the output of the force transducer was used as the feedback signal that feeds the servo-control system of the motor position.

2.2.3 Solution exchange apparatus

Fibres were activated by temperature jump using a solution exchange apparatus driven by a stepper motor (Linari *et al.*, 2007), which allows rapid change of temperature of the bathing solution to minimize the development of sarcomere non-uniformities due to the diffusion-limited time of activation across the fibre. The system consists of a movable platform carrying two aluminum plates that can be maintained at two different temperatures by means of two separated servocontrolled thermoelectric modules. Each plate carries two pedestals for the drops of solution confined between a bottom coverglass slit, stuck to the pedestal, and a top coverglass slit, stuck to a revolving arm. Upper and lower coverglasses 8 mm long and 3 mm wideare separated by 3 mm to have a final drop volume of ~ 70 µl (Fig. 19A).

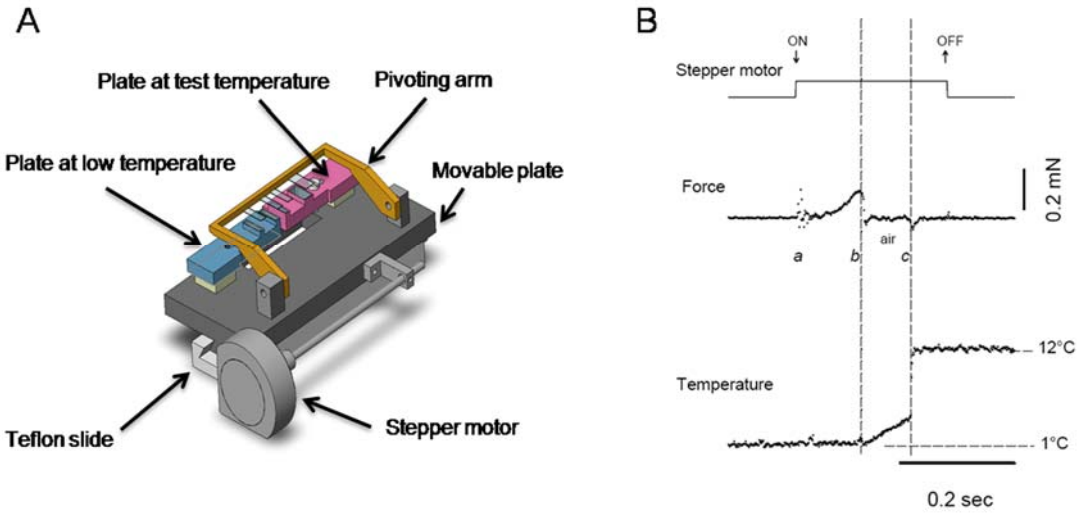

Figure 19. A. Schematic drawing of the experimental set-up. The blue and red colours of the plates indicate the low (blue) and test (red) temperature. The upper coverglasses are carried on a pivoting arm and can be removed to mount the fibre. **B.** Temperature change (lower trace) measured with a miniaturized (diameter 25 µm) fast thermocouple mounted in place of the fibre during the transition from the low temperature (1 °C) to the high temperature drop (12 °C). The top trace indicates stepper motor start (↓) and stop (↑), the middle trace is the force transducer signal. The artefacts in the force mark the start of the stepper motor motion for drop change (a) and the times when probe leaves the first (b) and enters the second drop (c). The time of travel in air (about 90 ms) is bounded by the vertical dashed lines. The temperature gradient in air is about 2.2 °C/mm, 30% of the temperature difference between the drops. The remaining 70% change in temperature occurs within 3-4 ms, at the interface of the high temperature drop.

The pedestals on the first plate (pedestal l and 2, blue in Fig. 19A) are used to transfer the fibre from relaxing solution to pre-activating and then activating solution kept at ~ 1 °C. In this way calcium

diffusion into the sarcoplasm occurs at a temperature at which development of high force is prevented. The pedestals on the second plate (violet) are used to transfer the fibre from activating solution at the test temperature (pedestal 3) to relaxing solution at the same test temperature (pedestal 4). When the activated fibre is transferred from pedestal 2 to pedestal 3 (4 mm apart), temperature rapidly changes from 1°C to the test temperature. In this way most of the force develops following the temperature jump, when calcium is homogenously distributed in the sarcoplasm, and the development of sarcomere non-uniformities is prevented.

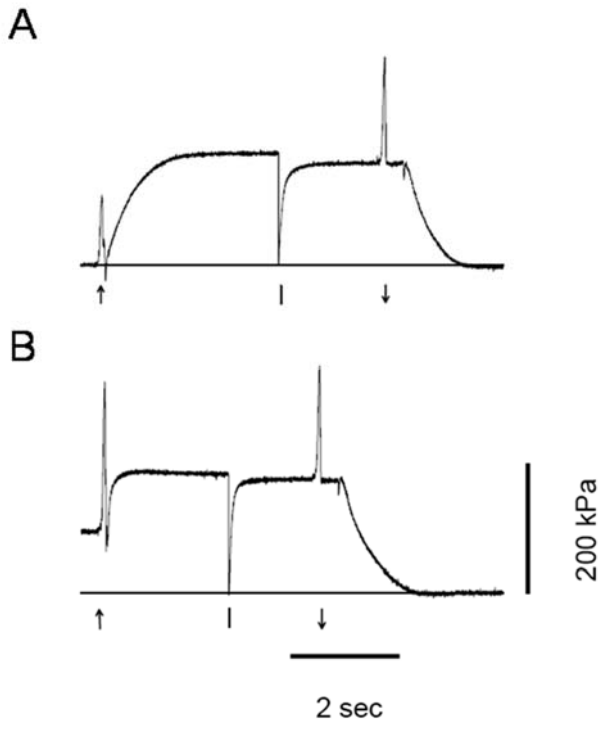

Figure 20. Force response to activation by Ca^{2+} at the test temperature **A** and at the low temperature followed by temperature jump **B**. The arrow (↑) indicates in (A) the transition from pre-activating to activating solution, in (B) the transition from low temperature to high temperature activating solution. A large release (about 8% of the initial fibre length, applied at the time marked in both panels by the vertical bar) was used to drop the force from the isometric force to zero. The arrow (↓) indicates the transition from activating solution to relaxing solution. The horizontal lines indicate zero force. Fibre length, 3.6 mm; average sarcomere length, 2.52 µm; CSA, 5740 μm^2.

The velocity of the temperature change, during the transfer from pedestal 2 (low temperature) to the pedestal 3 (test temperature), was measured with a miniaturized, unsheathed type K thermocouple (40.4 µV/°C, diameter 25 µm, chal-001, Omega Engineering Limited, Manchester, UK) mounted in place of the fibre, while the output signal was recorded with a monolithic thermocouple amplifier with cold junction compensation. As shown in Fig. 19B, for a temperature-jump from 1 to 12 °C, the temperature gradient in air is ~2.2 °C/mm and 70% of the temperature jump occurs sharply when the fibre enters the drop containing the solution at the test temperature. The heat capacity of the thermocouple and of the layer of the surrounding water makes the temperature jump complete in 3-4 ms. Thanks to this set-up the time needed to get half maximum force in the activating solution at the

test temperature is one order of magnitude faster in comparison to transferring the fibre from pre-activating solution to activating solution at the same temperature (Fig. 20).

2.2.4 Striation follower

The striation follower is an optoelectronic device similar to that previously described by (Huxley *et al.*, 1981) and composed of a light source (a 15 mW He-Ne laser, Melles Griot 05-LHR171, Carlsbad, CA, USA), a modified microscope mounted on a Zeiss ACM stand, and two photodiode arrays feeding analogue and digital electronics.

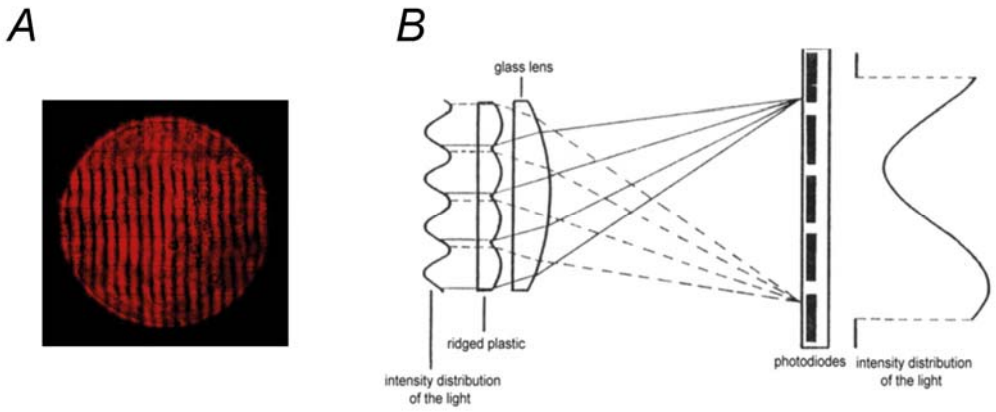

Figure 21. Striation follower. **A**: Image of the sarcomeres from one of the two regions at the level of the photodiode array. **B**: System for obtaining the optic average of the intensity distribution of several sarcomeres.

The instrument measures the longitudinal displacement of two separate regions of the fibre, each about 10 µm broad and containing six consecutive sarcomeres. A birefringent prism splits the laser beam in two beams that form two spots of 10 µm diameter; the rotation of the prism permits to set up the distance between the two regions in a range 0.5 – 3 mm. The angle of incidence of the illuminating beams is offset from the normal to the fibre axis so that the zero-order and only one first-order beam from each spot are collected by an objective (Leitz 10x, NA = 0.25) giving a simplified image of the sarcomeres as a sinusoidal intensity distribution of light. This distribution (magnified 2000x) is projected onto a plate with 6 cylindrical lenses mounted on the stage of the ACM stand, the height of which can be changed to have a sarcomere in each cylindrical lens. This is obtained by controlling the magnification with a 10x eyepiece (Zeiss, Germany), receiving part of the light distribution from a partially reflective prism, placed before the cylindrical lenses, that projects the image on a calibrated grid placed at the same distance as the lenses. The light distributions of the sarcomeres produced by the cylindrical lenses are superposed with a convergent lens forming a single light distribution representing the optical mean of the images of the six sarcomeres. This distribution is projected onto an array of five photodiodes, ranging from half the first to half the fifth (Fig. 21). The current signals

from the 5 photodiodes (I_1-I_5) are combined to give two output signals ($x = I_1+I_5-I_3$ and $y = I_2-I_4$) sensitive to the sinusoidal intensity distribution of the light due to sarcomeres and not to the intensity of the diffused light. The longitudinal movement of the fibre produces a variation of the intensity distribution expressed by $x = A\cdot\cos(2\pi\cdot D/\varphi)$ and $y = A\cdot\sin(2\pi\cdot D/\varphi)$, with D fibre displacement and φ average sarcomere length. Analogue and digital electronics collect the two signals from the two photodiode arrays, giving an output signal that measures the displacement of the region of the fibre in terms of sarcomere length with a precision of ~1% of the striation spacing and a time response of 1 μs, over a range of 128 sarcomeres. The displacements occurring at the level of the two regions are subtracted from each other so that the output signal gives the actual length change undergone by the selected fibre segment. The signal is converted into nm per half-sarcomere on the basis of the number of half-sarcomeres in the segment; consequently the error in the measurement of average length change per half-sarcomere is reduced by a factor corresponding to the number of the half-sarcomeres in the segment. The sensitivity was adjusted to 125 mV/nm per half-sarcomere.

The regions of interest in the fibre were selected on the basis of the quality of sarcomere image, by shifting longitudinally the movable stage and therefore the muscle fibre across the field of microscope objective.

Systematic errors may result from inhomogeneity of the sarcomere length within the segment and from changes of the sarcomere length in the laser spots on activation. The sarcomere inhomogeneity of the selected fibres was less than 5% at rest and those fibres developing gross inhomogeneity on activation were discarded.

2.3 Experimental protocol

A fibre segment, 4-6 mm long, was mounted between the lever arms of the loudspeaker motor and the capacitance force transducer in a drop of relaxing solution and, before starting the experiment, its extremes, clamped by T-clips, were fixed first with a rigor solution containing glutaraldehyde (5% v/v) and then glued to the clips with shellac dissolved in ethanol (8.3% w/v; (Bershitsky & Tsaturyan, 1995; Linari *et al.*, 1998). This procedure prevents the sliding of the ends of the fibre segment inside the clips and minimizes the shortening of the activated fibre against the damaged sarcomeres, at the ends of the segment, during the development of force. Afterwards the sarcomere length (*SL*), width (*w*) and height (*h*) were measured at 0.5 mm intervals in the central segment of the fibre (2-4 mm). The *SL* was adjusted to 2.4-2.6 μm, that is within the plateau region of the force-sarcomere length relation (Stephenson & Williams, 1982). The fibre cross sectional area (CSA) was determined assuming the cross-section as elliptical ($CSA = \frac{\pi}{4}\cdot w\cdot h$). The CSA ranged between 5000 and 7400

μm^2 in soleus fibres and between 3600 and 5700 μm^2 in psoas fibres. The CSA was 42% (slow fibres) and 38% (fast fibres) larger in the absence of dextran. Fibres were activated by temperature jump using the solution exchange system described above (Linari *et al.*, 2007). The fibre was kept in activating solution at the test temperature (12°C) for 3-5 seconds for the mechanical measurements. The striation follower allowed nanometer-microsecond resolution recording of length changes in a selected population of sarcomeres (range 500-1200 sarcomeres) starting at the time the optic path was permitted through the glass window in the floor of the test temperature drop (see Fig. 22A and B and (Linari *et al.*, 2007) for details).

2.3.1 Half-sarcomere stiffness measurements

To measure the stiffness of the half-sarcomere (hs), step length changes (ranging from -4 to +4 nm per hs, stretch positive), completed in 110 μs, were imposed on the isometrically contracting fibre. Half-sarcomere stiffness was estimated by the slope of the relation between the tension attained at the end of the step and the change in sarcomere length (T_1 relation). To enhance the precision of hs-stiffness measurements, a train of different-sized steps at 200-ms intervals was applied during each activation and, to maintain constant the isometric tension before the test step, each test step was followed, after a 50-ms pause, by a step of the same size but opposite direction (see Fig. 23A).

2.3.2 Contribution of myofilament compliance

The contribution of myofilament compliance to the half-sarcomere compliance was estimated by determining the relation between half-sarcomere strain and Ca^{2+}-modulated force. Under these conditions the changes in force are accounted for by the change in the number of interacting motors and the half-sarcomere strain depend solely on myofilament compliance.

2.3.3 Stiffness measurements in rigor

Rigor was induced by MgATP depletion at low temperature (1 °C) (Linari *et al.*, 2007). Stiffness was measured at different steady forces, similar to those developed by activated fibres at different pCa's, obtained by slowly stretching the rigor fibre starting from the low level of force (about 0.1 the isometric force attained at saturating pCa, $T_{0,4.5}$) developed at the end of the rigorization procedure to the desired force level. Measurement of hs-stiffness was done by applying the same

protocol as that used for activated fibres (see Fig. 23B).

2.3.4 Isotonic velocity transients

To measure the size and the speed of the working stroke, isotonic velocity transients in force clamp mode have been elicited by imposing stepwise drops to different fractions of the steady isometric force ($T_{0,4.5}$) attained on a fully activated fibre (pCa 4.5). To account for the artefacts in the force transducer signal due to the change of both temperature and solution, zero force in the test solution was measured by imposing, a large rapid shortening (6% L_0), 50 ms after the fibre entered the test-temperature activating solution. Force redeveloped from the slack and, once the isometric force had attained the plateau value, the control was shifted from fixed-end mode to force-clamp mode. Twenty milliseconds later, a drop in force, completed within 120–150 μs, was imposed by using as a command signal the output of an integrated circuit that generated steps to preset fractions of $T_{0,4.5}$. When the isotonic shortening had attained ~60 nm/hs, the control was shifted back to fixed-end mode and the motor was returned to its original position by a slow exponential. In force-clamp mode only the direct component of the force signal was used for the feedback, while the velocity component was taken from the motor lever position sensor. At any clamped force, several trials were necessary to adjust the gains of direct, velocity and lag amplifiers to optimise the force step.

2.3.5 Myosin isoform identification

The fibre type was defined on the basis of MHC isoforms used as molecular markers. The MHC isoform composition of each fibre used for the mechanical experiment was determined by means of 8% polyacrylamide gel electrophoresis after denaturation in sodium dodecyl sulphate (SDS-PAGE), following the procedure described by (Talmadge & Roy, 1993). In agreement with previous work (Tikunov *et al.*, 2001), the gel shows only one band in the region of MHC for each fibre, corresponding to the slow MHC-1 for fibres from soleus and the fast MHC-2X for fibres from psoas (Fig. 22C).

2.4 Data collection and analysis

Force, motor position and sarcomere length signals were recorded with a multifunction I/O board (PCI-6110E, National Instruments). A program written in LabVIEW (National Instrument) was

used for signal generation and data acquisition. Data analysis was performed using OriginPro 8.0 (OriginLab Corporation) and programs written in LabVIEW. Data are expressed as mean ± SEM. Force has been normalized for the CSA of the skinned fibre in relaxing solution with dextran.

2.5 Solutions

The composition of the solutions (Table 1) was calculated with a computer program similar to that described by (Brandt *et al.*, 1972) and (Goldman *et al.*, 1984). Cysteine and cysteine/serine protease inhibitors (trans-epoxysuccinil–L–leucylamido–(4–guanidine) butane, E – 64, 10 μM; leupeptin, 20 μg/ml) were also added to all solutions, in order to preserve lattice proteins and thus sarcomere homogeneity. The control solution contains ~1 mM Pi from two sources: Pi contamination in the experimental buffer and accumulation of Pi inside the fibre during contraction (Pate & Cooke, 1989).

The activating solution at a given pCa (range 6.8-4.5) was obtained by mixing relaxing and activating solutions.

A. Solution used during the experiments								
	Na_2ATP	$MgCl_2$	EGTA	HDTA	CaEGTA	TES	Na_2CP	GSH
relaxing	5.44	7.7	25	-	-	100	19.11	10
pre-activating	5.45	6.93	0.1	24.9	-	100	19.49	10
activating	5.49	6.76	-	-	25	100	19.49	10
rigor	-	3.22	53	-	-	100	-	10
B. Solution used to prepare and store skinned fibres								
	Na_2ATP	$MgCl_2$	EGTA	Imidazole	KP	NaN_3	PMSF	Glycerol
skinning solution	2.5	2.5	5	10	170	-	0.1	-
storage solution	2.5	2.5	5	10	170	5	-	50%

Table 1. Composition of solutions. All concentrations are in mM except glycerol (v/v). ATP, adenosine 5'-triphosphate; EGTA ethylene glycol-bis (β - aminoethyl ether)-N,N,N',N'-tetraacetic acid; HDTA, 1,6 diaminohexane-N,N,N',N'-tetraacetic acid; TES, N-tris[hydroxymethyl]methyl-2-aminoethanesulphonic acid; CP, phosphocreatine disodium salt Hydrate; GSH, glutathione, KP, potassium propionate; PMSF, phenylmethylsulphonyl fluoride. 1 mg/ml creatine phosphokinase, 10 μM trans-epoxysuccinyl-L-leucylamido-(4. guanidino) butane (E-64) and 20 μg/ml leupeptin, were added to all solutions. pH (adjusted with KOH) was 7.1 at the different temperature used (A), and 7.0 at 20 °C (B). Ionic strength ranged between 188 and 195 mM; free Mg^{2+} was 1.3 mM and MgATP was 5mM. HDTA was obtained from Fluka (Buchs, Switzerland), all other chemicals from Sigma.

Chapter 3 - Results

3.1 Isometric force development

As shown in Fig. 22, following a temperature-jump from 1°C to 12°C imposed in the activating solution at saturating [Ca^{2+}] (pCa 4.5), the force rose to a steady value ($T_{0,4.5}$), which, relative to the force developed at low temperature, is about 10 times larger in the slow fibres and about 3 times larger in the fast fibres (lower traces in Fig. 22A and B).

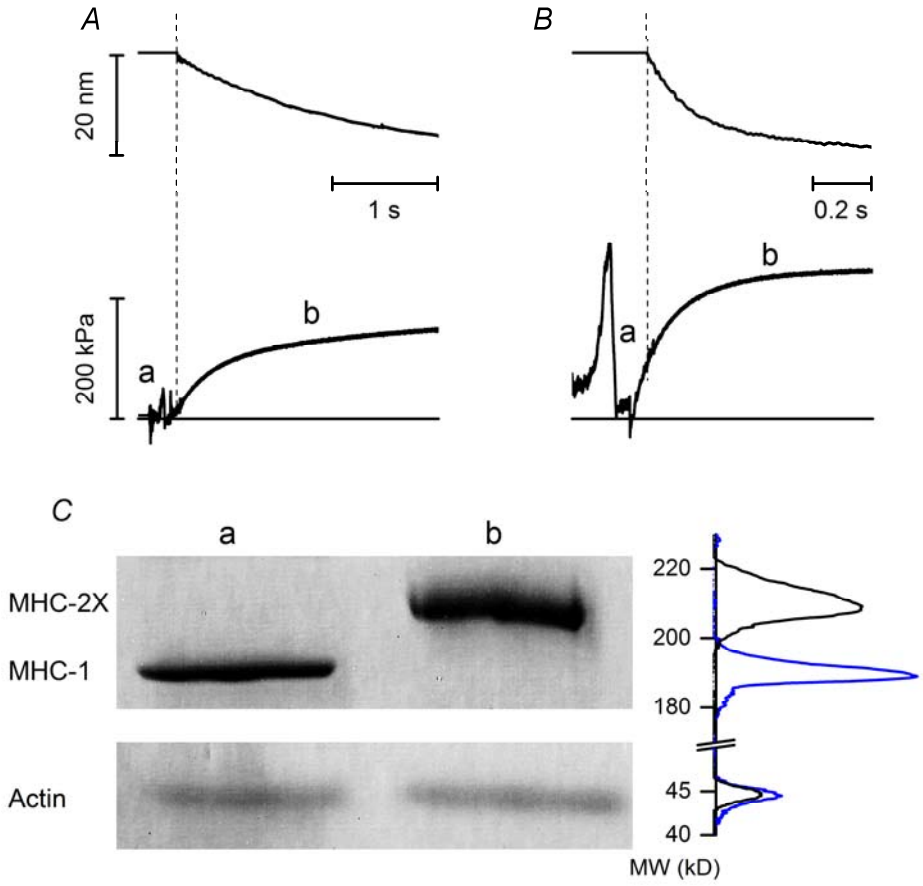

Figure 22. Force development following a T-jump (from 1 to 12°C) in slow (A) and fast (B) fibres and identification of fibre types (C). A and B. Traces indicate hs length change (upper panels) and force response (lower panels). The horizontal line in the lower panels indicates zero force. During the period (a) the fibre travels in air and within the shadow zone of the chamber. The dashed vertical lines mark the start of the period (b) when the striation follower signal is recorded. Slow fibre, type 1 isoform (**A**): 5 mm; segment length under the striation follower, 1.1 mm, average segment sarcomere length, 2.48 µm, test temperature, 12.5°C. CSA 5000 µm^2. Fast fibre, type 2X isoform (**B**): fibre length, 5.2 mm; segment length under the striation follower, 0.9 mm; average segment sarcomere length, 2.46 µm; CSA, 5700 µm^2. **C.** MHC isoform identification in the fibre by SDS-PAGE in the area of migration of myosin heavy chain (upper panel) and actin (lower panel). Lane a: single fibre from soleus muscle, which shows pure MHC-1content; lane b: single fibre from psoas muscle, which shows pure MHC-2X content. On the right of the lanes are shown the projections of the mass density along the vertical axis after horizontal integration: blue, slow fibre, and black, fast fibre.

The signal recording the sarcomere length change (upper traces) started with a delay with respect to the force developed at the test temperature, due to the time taken by the fibre travelling in the test temperature drop to get into the field of view of the striation follower. A similar difference between slow and fast fibres is observed in the time course of the force redevelopment after a period of unloaded shortening. The half-time of force redevelopment, $t_{1/2}$, was 413 ± 4 ms in the slow fibres (n=7) and 48 ± 1 ms in the fast fibres (n=8). The reciprocal of $t_{1/2}$ (k_{TR}) is 2.42 ± 0.02 s^{-1} in slow fibres and 20.9 ± 0.6 s^{-1} in fast fibres. $T_{0,4.5}$ was 264 ± 8 kPa in fast fibres and 141 ± 13 kPa, about one half of that in fast fibres. At the end of the experiment the MHC isoform composition was determined by SDS-gel electrophoresis (Fig. 22C): within the limit of precision of the method used here, slow and fast fibres contain pure isoforms, MHC-1 and MHC-2X respectively.

3.2 Half-sarcomere stiffness and motor strain in isometric contraction at different pCa

Slow and fast fibres were activated under isometric conditions at different [Ca^{2+}] (pCa range, 6.8-4.5). For each T_0 the half-sarcomere stiffness (k_0) was determined by superimposing on T_0 length steps in the range +4 to -4 nm per hs (Fig. 23A and left column in Fig. 24A).

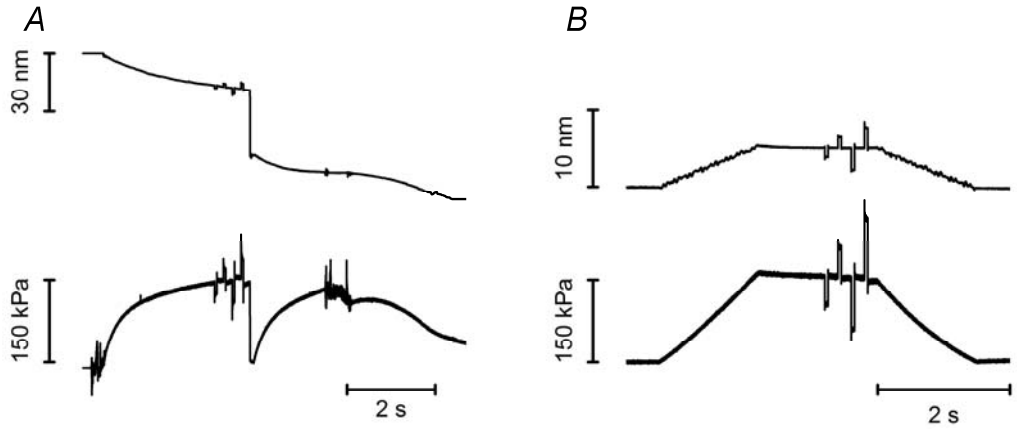

Figure 23. Protocol for measuring the stiffness of a slow fibre during isometric contraction at saturating [Ca^{2+}] (A) and at similar force in rigor (B). Upper trace, length change per half-sarcomere; lower trace, force. The same step sequence was imposed on both activated and rigor fibre. Step amplitudes in the sequence were: -1.5 nm; +1.5 nm; -3.0 nm; + 3.0 nm per hs. A step of opposite direction was imposed 50 ms after each test step to return the length and the force close to their values before the step. The interval between the test steps was 200 ms. Force is expressed relative to the CSA in relaxing solution (5150 μm^2). Fibre length, 5.3 mm; segment length under the striation follower, 0.93 mm, average segment sarcomere length, 2.45 µm, test temperature, 12.2 °C. For rigor (same fibre), average segment sarcomere length, 2.42 mm; temperature, 12.1 °C; CSA, 4030 μm^2.

k_0 was estimated as the slope of the relation between the force attained at the end of the steps and the size of the steps (T_1 relation, open circles in Fig. 24B for a slow fibre and C for a fast fibre). The rightward shift of the abscissa intercept of the linear fit to the T_1 relation (dashed lines) indicates that

k_0 decreases with the reduction of T_0 less than in proportion to force in both slow (open symbols in B) and fast (open symbols in C) fibres.

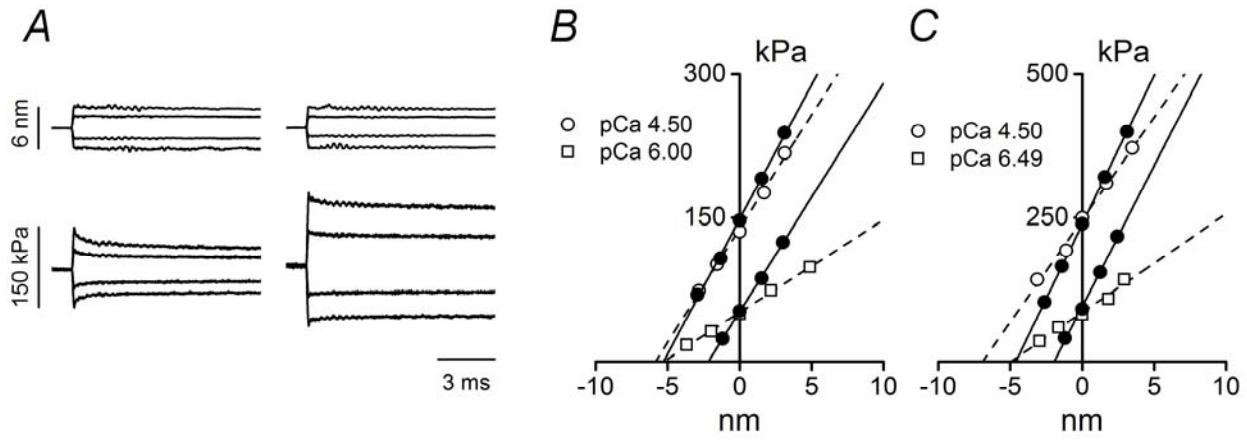

Figure 24. Measurements of the half-sarcomere stiffness during isometric contraction and in rigor in slow and fast fibres. A. Superimposed hs length changes (upper traces) and force response (lower traces) for steps of different sizes in a slow fibres activated at saturating [Ca^{2+}] (left column) and in rigor (right column) at a force about $T_{0,4.5}$. **B** and **C.** T_1 relations at different pCa (open symbols) and in rigor at about $T_{0,4.5}$ and 1/3 *$T_{0,4.5}$ (filled symbols) determined in a slow (B) and in a fast (C) fibres. Lines are linear regression equations fit to the active (dashed) or rigor (continuous) data. The abscissa intercept of each line is the average strain of the half-sarcomere before the length step (Y_0).

This reflects on the k_0-T_0 relations shown in Fig. 25A, where the points for both fast fibres (open circles) and slow fibres (filled circles) show an upward deviation with respect to their respective straight lines drawn from $T_{0,4.5}$ to the origin (continuous line, slow fibres, and dashed line, fast fibres). The reciprocal of k_0, C_{hs}, shows a hyperbolic-like dependence on force (Fig. 25B) for both slow (filled circles) and fast (open circles) fibres. At $T_{0,4.5}$ C_{hs} is 39.5 ± 6.0 nm/MPa in the slow fibres and 27.5 ± 2.5 nm/MPa in the fast fibres (Table 2). The hs strain Y_0, calculated as the product $C_{hs} \cdot T_0$, increases linearly with T_0 in slow (filled circles) and fast (open circles) fibres for forces > 40 kPa while it shows a downward concavity for forces < 40kPa (Fig. 25C).

Thus, in agreement with the finding in frog fibres during isometric force development (Fusi *et al.*, 2014), at forces > 40 kPa, the activated half-sarcomere can be reduced to a mechanical model where a motor array with the stiffness proportional to the number of attached motors is in series with an equivalent myofilament compliance (C_f) (Model 1, Fig. 11 in Introduction). In fact, in skinned fibres, the Ca^{2+} –dependent modulation of T_0 occurs through a corresponding change in the number of attached motors (Linari *et al.*, 2007). Thus the motor strain s_0 is constant independent of T_0 and Y_0 increases with force with a slope that is explained by the increase in the strain of the myofilaments with constant compliance C_f according to eqn (3):

$$Y_0(T_0) = C_f \cdot T_0 + s_0$$

The values of C_f and s_0, estimated by fitting eqn (3) to Y_0-T_0 values at forces > 40kPa (Table 2), did not differ significantly between slow (15.9 ± 1.0 nm/MPa and 3.33 ± 0.16 nm) and fast (15.1 ± 1.0 nm/MPa and 3.26 ± 0.20 nm) fibres (P > 0.5, Student's *t-test*).

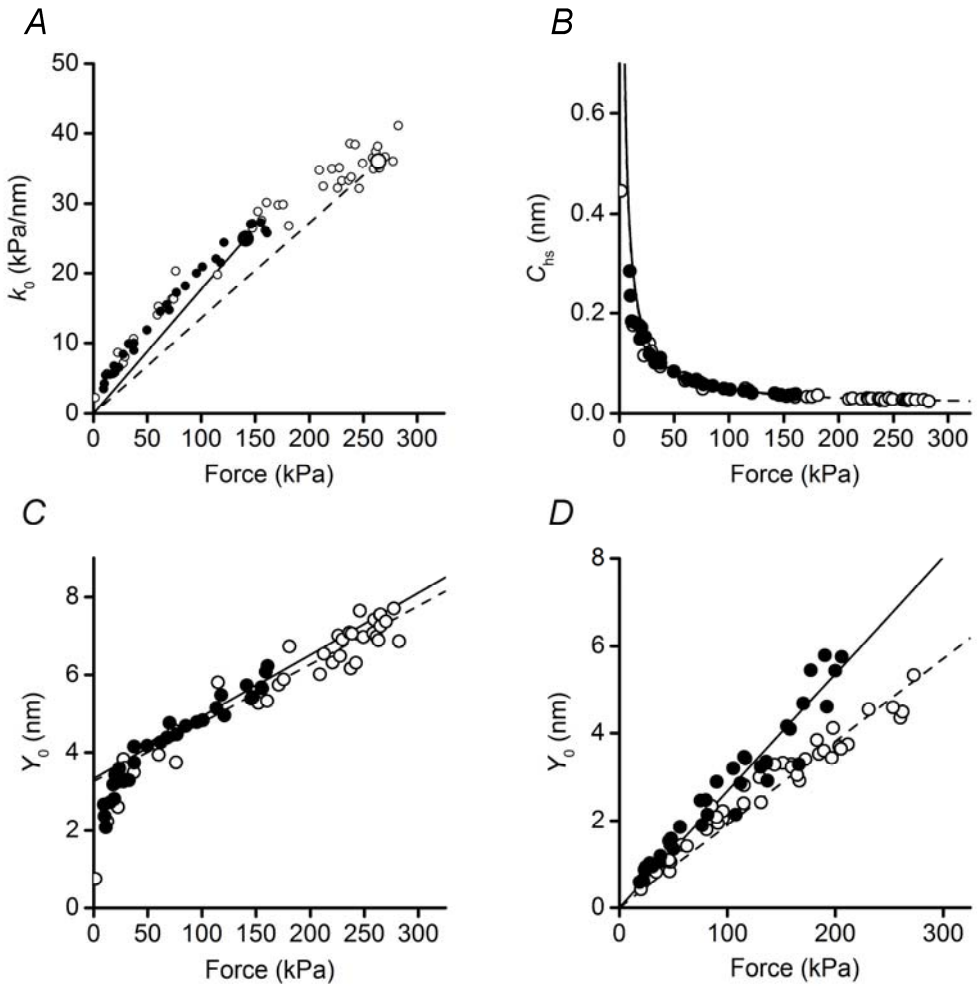

Figure 25. Half-sarcomere stiffness in isometric contraction and in rigor and derived parameters. A-C. Dependence on force of the hs-stiffness (A), hs-compliance (B) and hs-strain (C) in slow (filled circles) and fast (open circles) fibres. The lines in A are the linear extrapolations from the average $T_{0,4.5}$ (larger symbols) and the origin for slow (continuous line) and fast (dashed line) fibres. In B and C the lines are the calculated relations obtained under the assumption of a linear mechanical model of the hs (Model 1; continuous lines, slow and dashed lines, fast fibres). **D.** hs-strain relation in rigor in slow (filled circles) and fast (open circles) fibres. The lines are the linear regressions fit to data and forced to pass through zero (slow fibres, continuous line; fast fibres, dashed line).

Considering the whole range of the Y_0-T_0 data in Fig. 25C, a unique relation emerges for both slow and fast fibres with a downward concavity for forces < 40 kPa. A more detailed mechanical model of the half-sarcomere, where an elastic element in parallel the motor array explains the deviation from the linear relation (Model 2, Fig. 11 in Introduction), is expressed by the equation (4):

$$C_{hs}(T_0) = C_f + s_0 \cdot C_P/(s_0 + C_P \cdot T_0)$$

In Fig. 26, the fit of $C_{hs} - T_0$ relation with Model 2 (magenta line) is compared to the fit with Model 1 (black line) either for slow (A) or fast (B) fibres. The relevant parameters are reported in Table 3. The value of the compliance of the element in parallel with the myosin motors (C_P) does not depend

on fibre type: C_P is 589 ± 130 nm/MPa in the slow fibres and 539 ± 12 nm/MPa in the fast fibres. The estimates of C_f and s_0 with Model 2 do not differ from those calculated with Model 1.

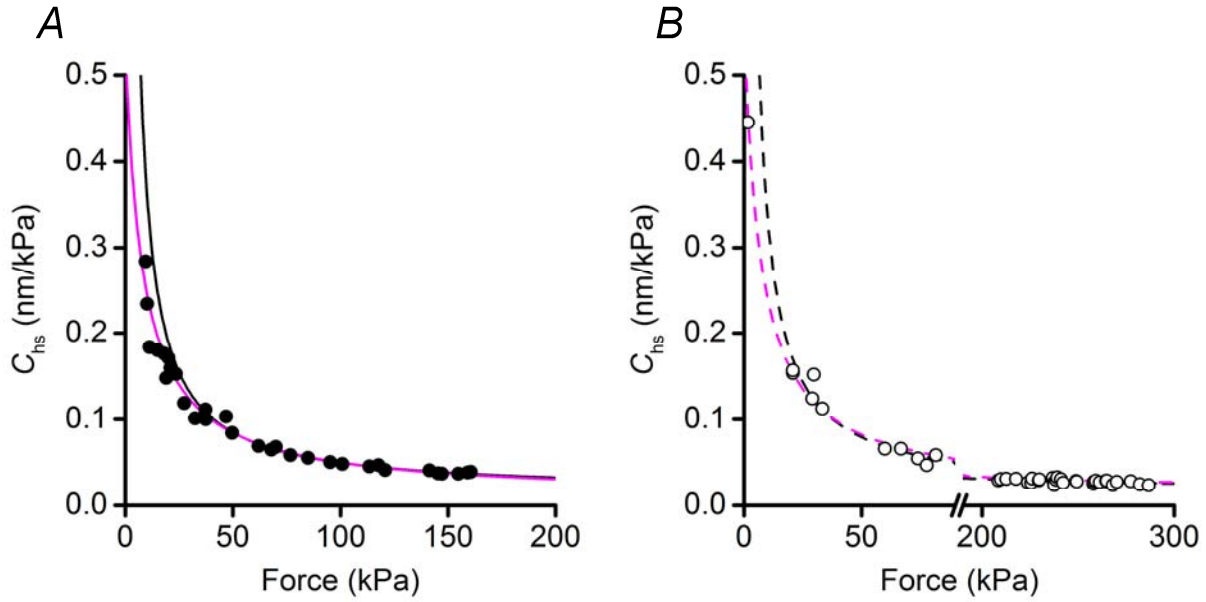

Figure 26. Dependence of the hs-compliance on force in slow (A) and fast (B) fibres. Experimental data are the same as those reported in Figure 24B. Lines in A and B represent the half-sarcomere compliance-isometric force relations calculated in the absence (black line, eqn (3) from Model 1) or in the presence (magenta line, eqn (4) from Model 2) of C_P, the elasticity in parallel with the myosin motors.

The above analysis shows that in both slow and fast fibres, as previously described during isometric development in frog fibres (Bagni *et al.*, 2002; Colombini *et al.*, 2010; Fusi *et al.*, 2014), the non-linear behaviour of the half-sarcomere elasticity at different [Ca^{2+}]-modulated isometric force can be explained by an elastic element in parallel with the array of myosin motors with a constant stiffness that is similar in both slow and fast fibres and is more than one order of magnitude larger than the compliance of the array of myosin motors working in parallel in the half-sarcomere at saturating [Ca^{2+}] in both slow and fast fibres. More precisely the ratio C_P/C_{cb} is (590/24 =) 24 in the slow fibres and (540/12 nm =) 45 in the fast fibres.

3.2.1 Half-sarcomere strain in rigor

The difference in $T_{0,4.5}$ between slow and fast fibres could be related to a different force of the myosin isoform and/or to a different number of motors attached to actin. Since the average strain of the motors at $T_{0,4.5}$ (s_0) is the same in both fibre types, a difference in the force per motor would imply a corresponding difference in motor stiffness. To clarify this point the half-sarcomere stiffness has been measured in rigor, a condition where all the myosin motors are attached to actin (Cooke &

Franks, 1980; Thomas & Cooke, 1980), so that any difference in the half-sarcomere stiffness between slow and fast fibres reflects a difference in stiffness between the myosin isoforms. The same step sequence as that used in activated fibres was applied to both slow and fast fibres in rigor to measure the half-sarcomere stiffness (Fig. 23B and right column in Fig. 24A). Different levels of steady force T (range 0.1-1.2 $T_{0,4.5}$) were attained by slowly stretching the rigorized fibres by different amount (L, 2–10 nm per hs). The T_l relations are shown by filled symbols in Fig 24B (slow fibres) and C (fast fibres). Considering that the number of myofilaments per fibre is the same independent of the reduced CSA in rigor, force has been normalized to the CSA of the relaxed fibre. The hs stiffness in rigor (k_r, measured by the slope of the T_l relation) is larger than in the activated fibre (open symbols), as expected because in the isometric contraction only a fraction of the myosin motors is attached to the actin filament. Furthermore, k_r is larger in the fast fibres than in the slow fibres and, within the same fibre type, k_r is independent of T, as shown by the parallel rightward shift of the T_l relations as force is reduced. Consequently, in the whole range of rigor forces considered, Y_0 increases in proportion to T (Fig. 25D, slow fibres, filled circles and fast fibres, open circles), as expected in rigor where all the elastic components of the half-sarcomere, the myofilaments and the array of myosin motors, are strained in proportion to force, and the relation between the hs strain, Y_0 and the steady rigor force, T shows a larger slope in the slow fibres than in the fast fibres. The linear regression fit to the pooled Y_0 - T points (lines in Fig. 25D), gives a slope of 26.8 ± 0.5 nm/MPa for the slow fibres and 19.0 ± 0.3 nm/MPa for the fast fibres. The slope of the relation is the half-sarcomere compliance in rigor (C_{hsr}), thus C_{hsr} in slow fibres is 41% larger than in fast fibres, indicating that the slow myosin isoform has a larger compliance than the fast myosin isoform.

The compliance of the motor array ($1/e_r$) can be determined by subtracting C_f to C_{hsr} and is 11.3 ± 1.2 nm/MPa for slow fibres and 3.5 ± 1.0 nm/MPa for fast fibres. Correspondingly the stiffness of the motor array in rigor (e_r), is 88.5 ± 9.4 kPa/nm and 285.7 ± 81.0 kPa/nm respectively (Table 2). The stiffness per myosin motor (ε) can be determined by dividing e_r by the density of myosin motors in the half-sarcomere (n_{hs}). Taking a density of myofibrils of 0.83 (Mobley & Eisenberg, 1975), from the lattice geometry it possible to obtain a value for n_{hs} of $1.68*10^{17}$ m^{-2} (calculated by multiplying the density of the thick filaments, $0.69*10^{15}$ m^{-2}, by the number of motors in the half-sarcomere, 294). In the slow isoform ε is 0.53 ± 0.06 pN/nm, while in the fast isoform ε is 1.70 ± 0.48 pN/nm (in agreement to the value reported by (Linari *et al.*, 2007). Thus ε is about three times larger in the fast than in the slow isoform.

3.3 Fraction of myosin motors responsible for active force

Since the average strain of the motors during an isometric contraction (s_0) is ~3.3 nm independently on the myosin isoforms, the finding that the stiffness of the slow motor isoform is three times smaller than that of the fast isoform implies that F_0, the average force developed by the motor in isometric contraction is three times lower in the slow isoform. In fact F_0 ($=\varepsilon \cdot s_0$) is 1.75 ± 0.52 pN in the slow isoform and 5.61 ± 1.60 pN in the fast isoform. In the slow fibres $T_{0,4.5}$ is only two times smaller than in the fast fibres, suggesting that the fraction of motors attached in the slow fibres (β) is larger than in the fast fibres to partly counteract the three times smaller force per motor. β can be determined by the ratio between the force per myosin motor if all myosin heads were assumed to be attached in the half-sarcomere, F_{hs} ($=T_{0,4.5}/n_{hs}$) and F_0. F_{hs} is 0.84 ± 0.08 pN in the slow isoform and 1.57 ± 0.05 pN in the fast isoform. β ($=F_{hs}/F_0$) is 0.48 ± 0.07 for the slow fibre and 0.28 ± 0.08 for the fast fibre.

Table 2. Estimate of the mechanical parameters of the half-sarcomere and of the myosin motor in slow and fast fibres. A. Measured parameters; B. Lattice geometry and force per myosin head site; C. Fraction of attached myosin motors and derived parameters.

MHC isoform	units	MHC-1	MHC-2X
A			
Isometric force (T0)	(kPa)	141 ± 13	264 ± 8
Filament compliance (Cf)	(nm/MPa)	15.9 ± 1.0	15.1 ± 1.0
Hs compliance in activated fibres	(nm/MPa)	39.5 ± 6.0	27.5 ± 2.5
Hs compliance in rigor	(nm/MPa)	26.8 ± 0.5	19.0 ± 0.3
Myosin head strain	(nm)	3.33 ± 0.16	3.26 ± 0.20
B			
Myosin to myosin spacing*	(nm)	41	
Myofibrillar volume density**	(%)	83	
Myosin head sites	(m^{-2})	$1.68 \cdot 10^{17}$	
Force per myosin head	(pN)	0.84 ± 0.08	1.57 ± 0.05
C			
Proportion of attached motors		0.48 ± 0.07	0.28 ± 0.08
Force per attached motor head	(pN)	1.75 ± 0.52	5.61 ± 1.60
Stiffness of the myosin motor	(pN/nm)	0.53 ± 0.06	1.70 ± 0.48

* value for mammalian skeletal muscle reported by Zappe and Maeda (1985), whole muscle from soleus and EDL, and for skinned fibres from psoas muscle after addition of 4% dextran to relaxing solution (Brenner & Yu, 1991; Kawai *et al.*, 1993).

** to my knowledge this value has not been reported for soleus and psoas muscle fibres from rabbit and it has been assumed to be the same as that reported for frog muscle (Mobley & Eisenberg, 1975) in both muscle types. The similarity of this value is suggested from data in literature for mouse muscles, where the myofibrillar volume density is 81% for soleus (slow) and 75% for EDL (fast) (Fig. 17 in (Luff & Atwood, 1971).

Table 3. Estimate of the mechanical parameters of the half-sarcomere with Model 1 and 2 in slow and fast fibres.

Model	**Slow fibres**			**Fast fibres**		
	s_0 (nm)	C_f (nm/MPa)	C_P (nm/MPa)	s_0 (nm)	C_f (nm/MPa)	C_P (nm/MPa)
Model 1	3.33 ± 0.16	15.9 ± 1.4		3.26 ± 0.20	15.1 ± 1.0	
Model 2	3.67 ± 0.53	15.3 ± 6.0	589 ± 130	3.45 ± 0.14	15.2 ± 2.0	539 ± 12

3.4 Size and speed of the working stroke in slow muscle fibres

The isotonic shortening following a stepwise drop in force imposed on a demembranated slow fibre during isometric contraction at saturating Ca^{2+} exhibits several phases (Fig. 27A), similar to those described in intact frog muscle fibres (Piazzesi *et al.*, 2002) and demembranated fast fibres (Fig. 27B, (Caremani *et al.*, 2013)) but, in general, the kinetics of the different phases is one order of magnitude slower. The first phase (phase 1) consists of a shortening simultaneous with the drop in force, due to the half-sarcomere elasticity, followed by phase 2, the early shortening phase, which is attributed to the synchronous execution of the working stroke in the attached myosin motors. The merging between the end of phase 1 and phase 2 might result in an overestimation of the elastic response at the expenses of the working stroke response (Piazzesi *et al.*, 2002). Therefore to estimate the size of phase 1 (L_1), the contribution of phase 2 to phase 1 is subtracted by back-extrapolating, to the force step half-time ($t_{1/2}$, vertical dashed line), the tangent to the initial part of phase 2 (magenta line). L_1 increases with the size of the force step and the relation between L_1 and the force attained at the end of the force step (L_1 relation, circles in Fig. 28A) can be fit with a linear regression equation that intercepts the ordinate at a value, 6.39 ± 0.22 representing the strain in the half-sarcomere at T_0, Y_0, not significantly different from that determined with the isometric force transient (Fig. 24B). Phase 2 following the elastic response has a roughly exponential time course and its size can be estimated by subtracting, from the length trace, the linear back extrapolation of the phase 3 shortening trace to $t_{1/2}$ (dotted line in Fig. 27 A and C).

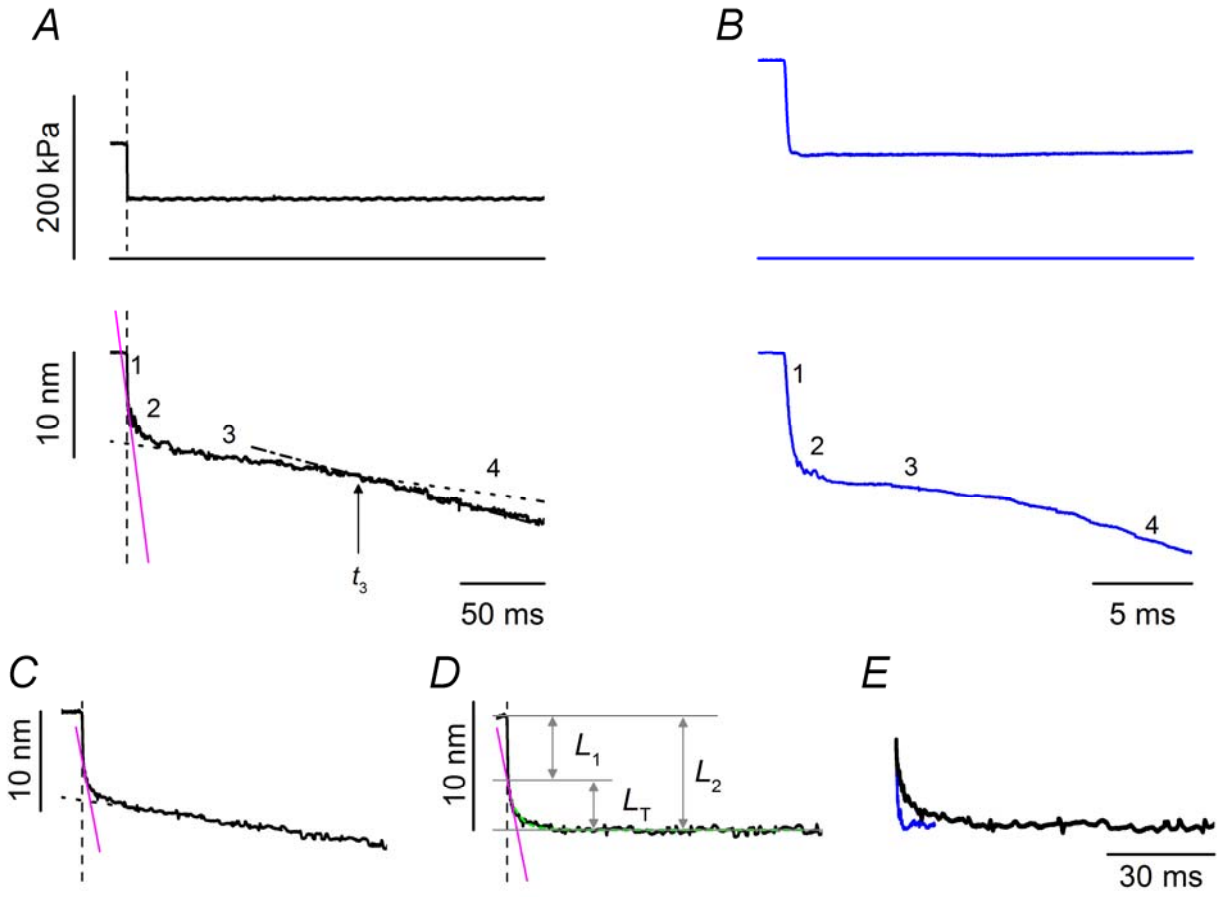

Figure 27. Isotonic velocity transient elicited in slow (A) and fast (B) fibres. In A and B is shown the shortening of the half-sarcomere (lower trace) in response to the step to 0.5 $T_{0,4.5}$ (upper trace). Numbers above the shortening record identify the phases of the transient; t_3 marks the transition between phases 3 and 4. **C** and **D**, early components of the shortening showing the method for estimating L_1 and L_2. L_1 is measured by extrapolating the tangent to the initial part of phase 2 response (magenta line) back to the half-time of the force step ($t_{1/2}$, indicated by the vertical dashed line). L_2 is measured by extrapolating the ordinate intercept of the tangent to the phase 3 response (dotted line) back to $t_{1/2}$. Alternatively, as shown in D, the whole time course of phase 2 shortening leading to L_2 is calculated by subtracting the phase 3 tangent from the record starting from $t_{1/2}$. L_T, the size of the working stroke, is obtained by subtracting the elastic response L_1 from L_2. Steady shortening velocity is estimated from the slope of the tangent to phase 4 response (dotted–dashed line in A) The green dashed line is the exponential fit to the trace starting from the end of the force step. **E.** Superposition of the time course of phase 2 in slow (black) and fast (blue) fibres. Slow fibre: fibre segment length, 6.3 mm; segment length under the striation follower, 0.65 mm; average sarcomere length, 2.31 μm; CSA, 2660 μm^2; temperature, 12.3°C; Fast fibre: fibre segment length, 3.3 mm; segment length under the striation follower, 1.0 mm; average sarcomere length, 2.51 μm; CSA, 3780 μm2; temperature, 11.8°C.

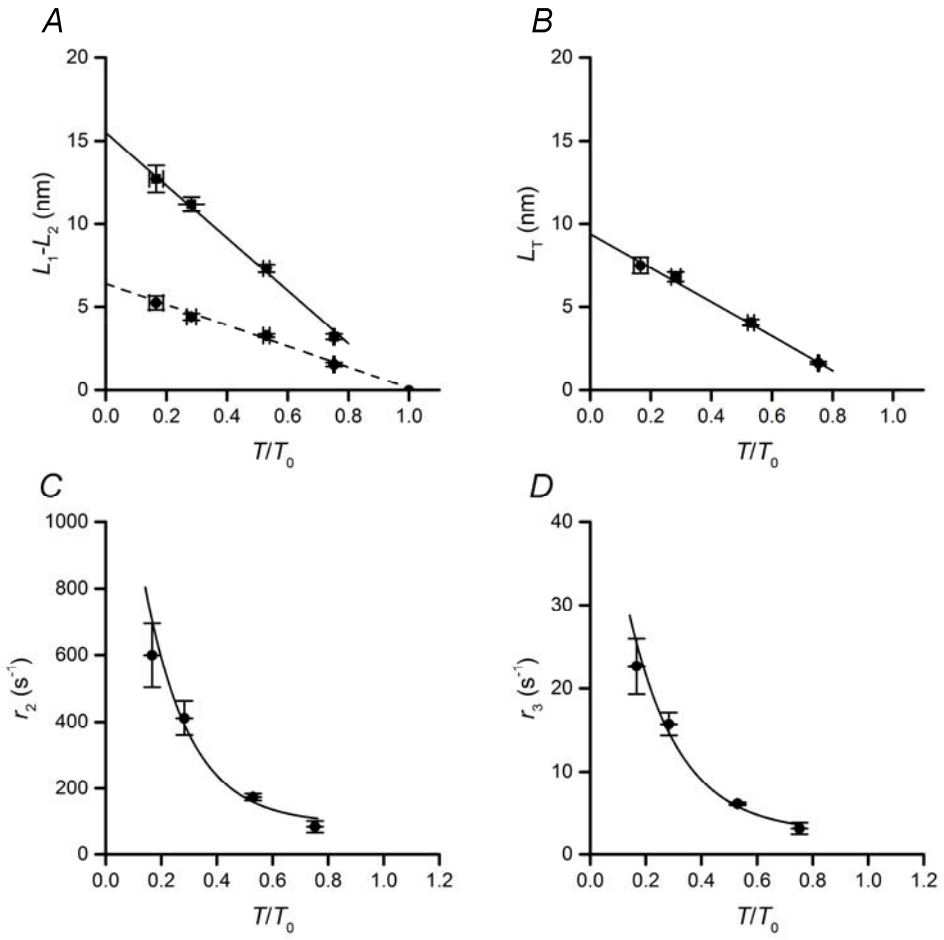

Figure 28. Force dependence of the parameters of phase 2 and phase 3 of the velocity transient in slow fibres. **A.** L_1 (circles) and L_2 (squares) relations. Lines are the linear regression fit to L_1 (dashed line) and L_2 (continuous line) data. **B.** L_T–force relation for the same experiments as in A. **C.** Rate of the isotonic working stroke (r_2) in relation to force. Line is the parabolic fit to data. **D.** Rate of phase 3 pause (r_3) in relation to force. In all graphs, T is relative to $T_{0,4.5}$. In each graph open symbols are data pooled from six fibres and filled symbols mean values ± SEM.

The distance between the horizontal trace obtained with the subtraction procedure and the length before the step estimates the total amount of shortening at the end of phase 2 (L_2). L_2 increases with the size of the force step and the L_2 relation (squares in Fig. 28A) can be fit with a line that intercepts the ordinate at 15.52 ± 0.64 nm/hs. This value represents the maximum amount of shortening accounted for by both the strain of the half-sarcomere elements (myofilaments and myosin motors) during the isometric contraction preceding the force step and the working stroke synchronized in the motors by the force drop. L_T, the amount of shortening accounted for by the working stroke of the myosin motors at the force T, is given by the difference ($L_2 - L_1$). L_T increases with the reduction of the load (Fig. 28B): it is 2 nm at 0.8 $T_{0,4.5}$ and increases up to 8 nm at 0.2 $T_{0,4.5}$. Assuming an exponential time course of phase 2 shortening in the trace of Fig 27D, the time elapsed between $t_{1/2}$ and the abscissa intercept of the tangent to the initial part of the trace (magenta line) is an estimate of the time constant of phase 2 shortening and its reciprocal is an estimate of the rate constant of the process (r_2) (green dashed line in Fig. 27D). r_2 increases roughly exponentially with the reduction of

the load (Fig. 28C) from 100/s at 0.8 $T_{0,4.5}$ to 600/s at 0.2 $T_{0,4.5}$. Phase 2 is followed by a pause in shortening (phase 3), which eventually evolves in a steady shortening at constant velocity (phase 4). The end of phase 3 is measured as the time (t_3) from $t_{1/2}$ to the intercept between the tangent to phase 4 shortening (dotted-dashed line in Fig. 27A) and the tangent to phase 3 (dotted line). The duration of phase 3, (τ_3), calculated by taking as starting point the end of phase 2 (estimated as $2*\tau_2$), decreases with the reduction of the load so that its reciprocal (r_3), an estimate of the rate of phase 3 motor detachment from actin following the execution of the working stroke, rises roughly exponentially with the reduction of the load (Fig. 28D). The final steady shortening occurs at a velocity defined by the force–velocity relation (phase 4, Fig. 29A). The curvature ($a/T_{0,4.5}$= 0.17 ± 0.08) and the ordinate intercept (the unloaded shortening velocity, V_0 = 0.28 ± 0.06 μm/s per hs) of the relation are estimated by fitting the hyperbolic Hill equation to data. The force-velocity relation is used to calculate the power (force x velocity) as a function of the load in Fig. 29B. The maximum power, obtained at about 1/3 $T_{0,4.5}$, is about 2.1 mW/g.

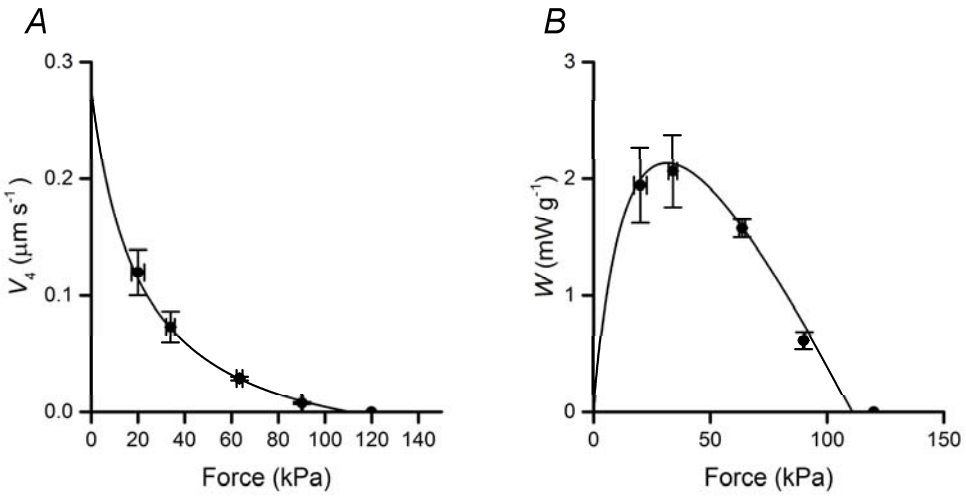

Figure 29. Force dependence of the parameters of phase 4 of the velocity transient. A. Relation between steady shortening in phase 4 (V) and force. **B.** Power–force relations calculated from the data in A (open circles, pooled data; filled circles, mean values ± SEM). Line in A is the fit to the data using the hyperbolic Hill equation. Line in B is calculated from the line in A.

Chapter 4 – Discussion

Fast sarcomere level mechanics in Ca^{2+}-activated skinned fibres from rabbit slow muscle (soleus), are used to define the properties of the slow myosin isoform as single motor (stiffness of the motor, size and the speed of the working stroke and its dependence on the load), as well as the ensemble properties in the half-sarcomere (fraction of motors attached in isometric contraction, kinetics underlying both isometric force development and force-velocity relation). The importance of the study emerges from the comparison of the relevant parameters with those from fibres of rabbit fast muscle (psoas) (expressing >90% the fast isoform MHC-2X).

4.1 Single motor properties

Stiffness and force of the motor.

In slow fibres (expressing >90% MHC-1) the stiffness per myosin motor is 0.53 pN/nm, about three times smaller than in fast fibres (1.70 pN/nm). According to the crystallographic model of force generation (Rayment *et al.*, 1993a) the stiffness between the catalytic domain attached to actin and the extremity of the lever arm that transfers force and movement to the thick filament is responsible for the gain in the coupling between the conformational change responsible for the working stroke and the produced force. A lower motor stiffness provides a lower force for the same conformational change. For the same average strain of the motor in isometric contraction (3.3 nm), the force developed by the slow isoform (~1.8 pN) is about one third of that developed by the fast isoform (~5.6 pN). The effect on the macroscopic force of the reduced motor stiffness in the slow fibres is attenuated by the larger number of myosin motors working in parallel in the half-sarcomere, therefore the force per cross sectional area developed by the slow fibres is about one-half of that developed by the fast fibres. With respect to the stiffness of the fast myosin isoform, the lower stiffness of the slow myosin isoform could also explain the smaller size of the working stroke during shortening at high-intermediate loads and its slower speed.

The isotonic velocity transient.

To compare the mechanokinetic properties of the motor (size and speed of the working stroke) determined in this work for the slow isoform with those determined for the fast isoform (Caremani *et*

al., 2013), it must be preliminarily taken into account that Caremani et al experiments were carried out in the absence of the osmotic agent dextran T-500 that recovers the original interfilamentary spacing. However, tests on fast fibres demonstrate that, for loads ranging between 0.2 and 0.8 $T_{0,4.5}$, the isotonic velocity transient is the same independent of the presence/absence of the osmotic agent (data not shown).

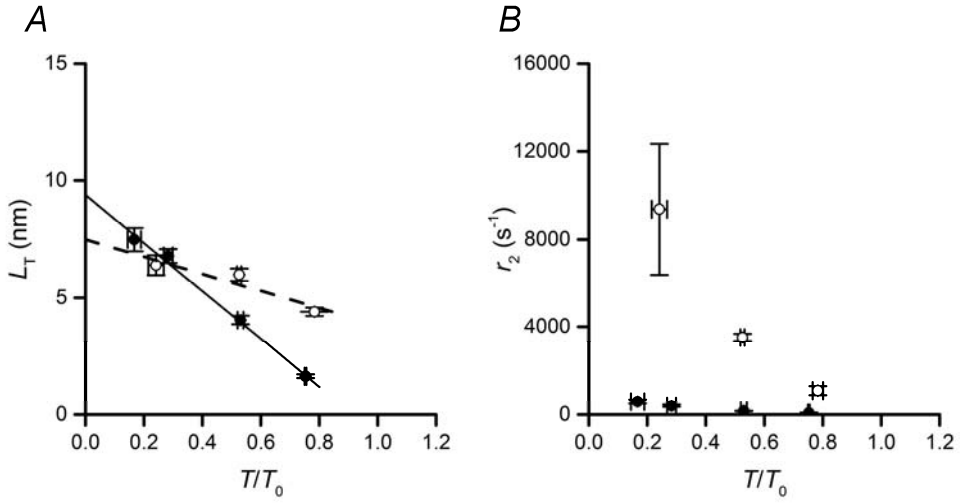

Figure 30. Comparison of the size (A) and rate (B) of the isotonic working stroke in slow and fast fibres. Slow fibres filled circles, fast fibres open circles. Data for fast fibres from (Caremani *et al.*, 2013).

At high load (0.8 $T_{0,4.5}$) the size of the isotonic working stroke (L_T) is smaller in the slow isoform (2 nm) than that in the fast isoform (5 nm), while it is similar at low load: at 0.2 $T_{0,4.5}$, L_T is 7-8 nm for both myosin isoforms (Fig. 30A). On the contrary, the rate of the working stroke (r_2) is one order of magnitude slower in the slow isoform with respect to the fast isoform at any load (Fig. 30B). At high load (0.8 $T_{0,4.5}$) r_2 of the slow isoform is 100/s, ten times slower than that of the fast isoform (~ 1000/s). Decrease in load from 0.8 to 0.2 $T_{0,4.5}$ increases r_2 by ~6 times independently of the myosin isoforms, so that the ten times difference in this kinetic parameter is maintained at all loads.
In conclusion in both isoforms the isotonic working stroke is larger and faster at low load. However the load dependence of the size of the working stroke is much more marked in the slow isoform. A corollary observation is that a similar load dependence of the size of the working stroke as that in the fast isoform (8-5 nm from low to high load) has been found in the twitch muscle of the frog (Piazzesi *et al.*, 2002).

Kinetic model of force generation.

According to the crystallographic model (Rayment *et al.*, 1993a) the working stroke in the actin attached motors produces a filament sliding of 11 nm, in quite good agreement with the predictions of Huxley and Simmons mechano kinetic model of force generation (1971). Huxley and

Simmons model provides that the attached motors exist in two force generating states and that the proportional occupancies of these states is governed by the load that contributes to the activation energy barrier of the forward transition. Actually it has been shown that, considering the relatively high stiffness of the motor determined after the formulation of the theory, several transitions are necessary to account for the 11 nm working stroke (Piazzesi & Lombardi, 1995; Piazzesi *et al.*, 2014). Here for simplicity three force generating states are assumed (A_1, A_2 and A_3), with a 5 nm progression in the working stroke for each of the two transitions A_1-A_2 and A_2-A_3. A drop in force reduces the mechanical energy barrier and promotes a forward transition, which accounts for the phase 2 of the isotonic velocity transient. Fig. 31 shows the free energy parabolic profiles of the three states and their dependence on *x* (the displacement of the myosin motor from the position at which the force in state A_1 is zero), calculated according to the different motor stiffness of the slow (A, 0.53 pN/nm) and fast (B, 1.7 pN/nm) isoforms.

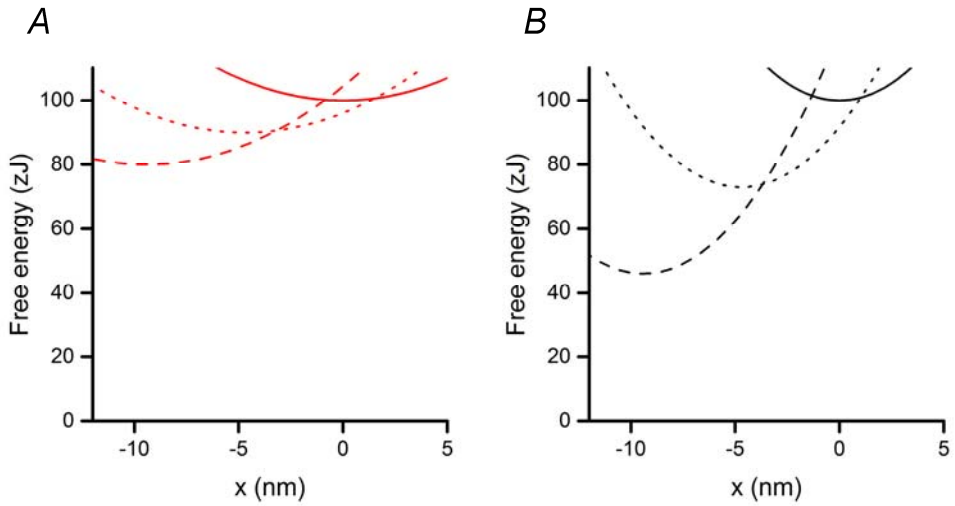

Figure 31. Free energy profiles of the attached states of the slow (A) and fast (B). *x*, displacement from the position at which the force in state A_1 is zero. The free energy curves (A_1 continous line, A_2 dotted line, A_3 dashed line) are positioned vertically so that in isometric contraction the fractional occupancy of states is 0.3 A_1 and 0.7 A_2 for both slow and fast fibres at 12°C. This constraint and the 5 nm step size determine the difference between the free energy minima.

The distance between the minima of the free energy curves (*z*,) is set to 5 nm to attain the completion of the working stroke with two steps and the fractional occupancies of A_1 (0.3) and A_2 (0.7) in isometric contraction at 12°C have been constrained by the temperature-dependence of force (Linari *et al.*, 2007). For the fast isoform the motor stiffness is 1.7 pN, so that the slope of the free energy parabolas provides a difference between the free energy minima of consecutive parabolas of 21 zJ. Thus the total free energy made available by the two transitions is 42 zJ, which fits the known efficiency of energy conversion in fast muscle (0.4-0.5), considering that the free energy of the ATP hydrolysis is 100 zJ (Barclay *et al.*, 2010a). The same assumptions, except for the stiffness, are used

for calculating the free energy change for the same 5 nm transition in the slow isoform. The result is a difference between free energy minima of consecutive parabolas of 6 zJ, and a total free energy made available by the two transition of 12 zJ (less than 1/3 of that of the fast isoform). A corresponding decrease in the efficiency of energy conversion is predicted. This conclusion, however, is not supported by the data reported in literature. In fact the efficiency in the slow fibres is similar to (Barclay *et al.*, 1993; He *et al.*, 2000) or higher than (Woledge, 1968; Barclay *et al.*, 2010b) that measured in fast fibres, suggesting the presence of a mechanism in slow myosin isoform able to recover the efficiency of energy conversion despite the lower stiffness.

4.2 Properties of the motor ensemble

Kinetics underlying the isometric contraction and the force-velocity relation.

The relevant parameters of the ensemble kinetics estimated in slow fibres during isometric contraction are the fraction of attached myosin motors (β) and the rate of force development (k_{TR}). Based on a simple two-state model of acto-myosin interaction (Huxley, 1957), β and k_{TR} are related to the apparent rate constant of attachment (f) and detachment (g) according to the following equations:

$\beta = f/(f+g)$ and $k_{TR}=f+g$

By knowing β and k_{TR}, f (=β *k_{TR}) and g (=k_{TR}*(1- β)) can be calculated and compared with those of fast fibres (Caremani et al., 2013). For slow fibres f and g are 5 and 12 times slower than in fast fibres, respectively. The reduction of f with fibre types is somewhat smaller than that reported in literature: it has been found that in slow fibres the forward rate constant of the force generating step is >40 times slower than in fast fibres (Millar & Homsher, 1992). Based on f and g values, the predicted ATP hydrolysis rate in isometric conditions ($k_{CAT}=f*g/(f+g)$) in slow fibres is 13% of that in fast fibres. The one order reduction in k_{CAT} is in quite good agreement with the experimental observations by (Potma *et al.*, 1995) that reported an isometric ATPase rate for the slow fibres 0.05 mM/s, that is 12% of that in fast fibres (0.41 mM/s). It is instructive to compare the kinetics of ATPase rate and liberation of ATP hydrolysis products in slow and fast fibres in relation to k_{CAT} under high load. The rate of hydrolysis of ATP measured in solution (step 2 in the ATPase cycle of Scheme 1 in Introduction) is the same for slow and fast myosin isoforms (Marston & Taylor, 1980) and, assuming that it is the same in skinned fibres because this step occurs in detached motors (Millar & Homsher, 1992), this

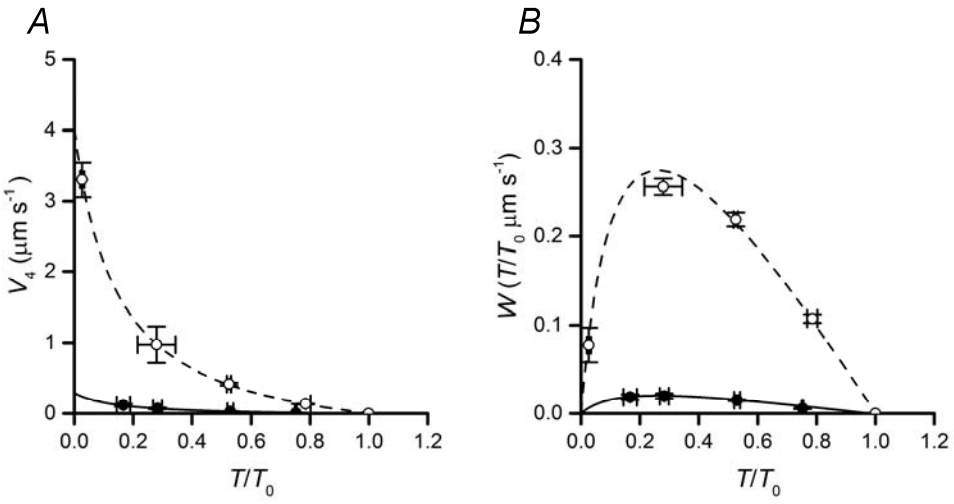

Figure 32. Force dependence of steady shortening velocity (A) and power (B) in slow (filled circles) and in fast (open circles) fibres. Fast fibres, data from (Caremani *et al.*, 2013).

step does not explain the lower ATPase rate in slow fibres. In fast fibres the release of Pi is a relatively fast process (Dantzig *et al.*, 1992) and k_{CAT} would be limited by the rate of ADP release (Linari *et al.*, 2010; Caremani *et al.*, 2015). On the contrary in slow fibres the rate of Pi release is a slow process (Millar & Homsher, 1992), suggesting that not only release of ADP but also release of Pi would limit k_{CAT}.

Comparison of the force-velocity relations in slow and fast fibres (Fig 32A) shows that at any relative load the steady shortening velocity is ten times smaller than in fast fibres. Consequently at the same relative load also the power is ten times smaller (Fig 32B). The maximum power (at 1/3 $T_{0,4.5}$) developed by the collective motor is 0.02 T/T_0 µm s^{-1} hs^{-1} for the slow isoform, about 1/10 of that developed by the collective motor of the fast isoforms (0.28 T/T_0 µm s^{-1} hs^{-1}).

Contributions of different structures to half-sarcomere elasticity.

The structural components that contribute to the hs elasticity are the thick and thin filaments, the array of myosin motors attached to actin and an element in parallel with motors (Ford *et al.*, 1981; Linari *et al.*, 1998; Bagni *et al.*, 2002; Linari *et al.*, 2007; Piazzesi *et al.*, 2007; Colombini *et al.*, 2010; Brunello *et al.*, 2014; Fusi *et al.*, 2014). The compliance of this element (C_P) is so large (~560 nm/MPa) that at forces > 40 kPa, its effect is negligible and the compliances of the other elements explain the whole hs compliance: $C_{hs} = C_f + 1/\beta\varepsilon$. In slow fibres C_f, measured by the slope of the hs strain-force relation, is 15.9 ± 1.0 nm/MPa, which is similar to that of fast fibres. The ordinate intercept of the relation measures the average strain in the attached myosin motor in isometric contraction (s_0, 3.33 nm) and also this parameter is similar to that measured in fast fibres.

At forces < 40 kPa, the hs strain reduces with the reduction of force more than expected from the

filament compliance, due to the presence of the parallel element with constant compliance C_P (~560 nm/MPa). C_P is so large that only when the number of attached motors is very low it contributes significatively to the hs elasticity. C_P is the same in slow and fast fibres, as expected from a parallel elasticity generated by a protein different from the myosin motor (likely titin or myosin-binding protein C). The value of C_P in demembranated fibres is about twice that found in intact fibres of the frog (Fusi *et al.*, 2014). Accordingly the contribution to stiffness at low force is much less marked in both slow and fast fibres. The difference is not eliminated with the use of the osmotic agent that in demebranated fibres recovers the interfilamentary spacig (Martyn *et al.*, 2002; Linari *et al.*, 2007; Seebohm *et al.*, 2009). This indicates that the larger C_P in skinned fibres from mammals with respect to intact fibres from amphibians could be related to the mechanical properties of the parallel elasticity *per se* or to a difference in the properties of the milieu surrounding the contractile material. Further experiments are necessary to clarify this point and identify the origin of C_P.

Stiffness of the myosin motor and amino acid sequence of the converter domain

The domain of the actomyosin complex that experiences the main elastic distortion is unknown. One possibility is that the long α-helix undergoes bending (Uyeda *et al.*, 1996; Dobbie *et al.*, 1998; Irving *et al.*, 2000) or, alternatively, the regions of major distortion could be the acto-myosin interface (Huxley, 1974) or the junction between catalytic domain and light chain domain (Dobbie *et al.*, 1998), the converter domain, as suggested by single amino acid mutations in this region (Kohler *et al.*, 2002; Seebohm *et al.*, 2009; Brenner *et al.*, 2014). In slow muscle fibres from soleus muscle of human it has been found that a single natural occurring mutation in the converter domain (708-780 region) of the slow β-MHC isoform is responsible for a large change in motor stiffness. In fact, when proline (K) in position 713 or valine (V) in the position 719 are replaced with tryptophane (T) the stiffness of the myosin motor increases 2-3 times (Kohler *et al.*, 2002; Seebohm *et al.*, 2009; Brenner *et al.*, 2014). Comparison of the available amino acid sequence of the converter domain between the slow and fast myosin isoforms of six species of mammals of different size (mouse, cattle, rabbit, pig, dog and human, Fig. 15 in Introduction), shows a difference in the amino acid contents of about 55% in rabbit, much larger than that found in the other species (16-20% difference). This makes impossible to relate the difference in motor stiffness between slow and fast isoforms to changes of few aminoacid within this region. On the other hand, the larger difference is related to the composition of the converter domain of the slow myosin isoform in rabbit with respect to the slow isoform of the other species while the converter domain of the fast myosin isoforms is well preserved among species. If the converter domain plays a major role in determining the motor stiffness, the stiffness of the fast myosin isoform should be similar in the different species while the

slow isoform would have different stiffness. Data in literature (Seebohm *et al.*, 2009) support this hypothesis: in fact, the motor stiffness measured in the slow myosin isoform from human is 0.3 pN/nm, 60% lower than that found in this work for rabbit.

References

Bagni MA, Cecchi G, Colombini B & Colomo F. (2002). A non-cross-bridge stiffness in activated frog muscle fibers. *Biophys J* **82,** 3118-3127.

Bang ML, Caremani M, Brunello E, Littlefield R, Lieber RL, Chen J, Lombardi V & Linari M. (2009). Nebulin plays a direct role in promoting strong actin-myosin interactions. *FASEB J* **23,** 4117-4125.

Barany M. (1967). ATPase activity of myosin correlated with speed of muscle shortening. *J Gen Physiol* **50,** Suppl:197-218.

Barclay CJ, Constable JK & Gibbs CL. (1993). Energetics of fast- and slow-twitch muscles of the mouse. *J Physiol* **472,** 61-80.

Barclay CJ, Woledge RC & Curtin NA. (2010a). Inferring crossbridge properties from skeletal muscle energetics. *Prog Biophys Mol Biol* **102,** 53-71.

Barclay CJ, Woledge RC & Curtin NA. (2010b). Is the efficiency of mammalian (mouse) skeletal muscle temperature dependent? *J Physiol* **588,** 3819-3831.

Bershitsky SY & Tsaturyan AK. (1995). Force generation and work production by covalently cross-linked actin-myosin cross-bridges in rabbit muscle fibers. *Biophys J* **69,** 1011-1021.

Bottinelli R, Canepari M, Pellegrino MA & Reggiani C. (1996). Force-velocity properties of human skeletal muscle fibres: myosin heavy chain isoform and temperature dependence. *J Physiol* **495 (Pt 2),** 573-586.

Bottinelli R, Schiaffino S & Reggiani C. (1991). Force-velocity relations and myosin heavy chain isoform compositions of skinned fibres from rat skeletal muscle. *J Physiol* **437,** 655-672.

Brandt PW, Reuben JP & Grundfest H. (1972). Regulation of tension in the skinned crayfish muscle fiber. II. Role of calcium. *J Gen Physiol* **59,** 305-317.

Brenner B, Seebohm B, Tripathi S, Montag J & Kraft T. (2014). Familial hypertrophic cardiomyopathy: functional variance among individual cardiomyocytes as a trigger of FHC-phenotype development. *Frontiers in physiology* **5,** 392.

Brenner B & Yu LC. (1991). Characterization of radial force and radial stiffness in Ca(2+)-activated skinned fibres of the rabbit psoas muscle. *J Physiol* **441,** 703-718.

Brunello E, Caremani M, Melli L, Linari M, Fernandez-Martinez M, Narayanan T, Irving M, Piazzesi G, Lombardi V & Reconditi M. (2014). The contributions of filaments and cross-bridges to sarcomere compliance in skeletal muscle. *J Physiol* **592,** 3881-3899.

Cambridge EW & Haines J. (1959). A new versatile transducer system. *J Physiol* **149,** 2-3P.

Caremani M, Melli L, Dolfi M, Lombardi V & Linari M. (2013). The working stroke of the myosin II motor in muscle is not tightly coupled to release of orthophosphate from its active site. *J Physiol* **591,** 5187-5205.

Caremani M, Melli L, Dolfi M, Lombardi V & Linari M. (2015). Force and number of myosin motors during muscle shortening and the coupling with the release of the ATP hydrolysis products. *J Physiol* **593,** 3313-3332.

Cecchi G. (1983). A circuit specially suited for use with high-frequency capacitance gauge force transducers. *Arch Ital Biol* **121,** 215-217.

Colombini B, Nocella M, Bagni MA, Griffiths PJ & Cecchi G. (2010). Is the cross-bridge stiffness proportional to tension during muscle fiber activation? *Biophys J* **98,** 2582-2590.

Cooke R & Franks K. (1980). All myosin heads form bonds with actin in rigor rabbit skeletal muscle. *Biochemistry* **19,** 2265-2269.

Dantzig JA, Goldman YE, Millar NC, Lacktis J & Homsher E. (1992). Reversal of the cross-bridge force-generating transition by photogeneration of phosphate in rabbit psoas muscle fibres. *J Physiol* **451,** 247-278.

Decostre V, Bianco P, Lombardi V & Piazzesi G. (2005). Effect of temperature on the working stroke of muscle myosin. *Proc Natl Acad Sci U S A* **102,** 13927-13932.

Dobbie I, Linari M, Piazzesi G, Reconditi M, Koubassova N, Ferenczi MA, Lombardi V & Irving M. (1998). Elastic bending and active tilting of myosin heads during muscle contraction. *Nature* **396,** 383-387.

Dominguez R, Freyzon Y, Trybus KM & Cohen C. (1998). Crystal structure of a vertebrate smooth muscle myosin motor domain and its complex with the essential light chain: visualization of the pre-power stroke state. *Cell* **94,** 559-571.

Fisher AJ, Smith CA, Thoden JB, Smith R, Sutoh K, Holden HM & Rayment I. (1995). X-ray structures of the myosin motor domain of Dictyostelium discoideum complexed with MgADP.BeFx and MgADP.AlF4. *Biochemistry* **34,** 8960-8972.

Ford LE, Huxley AF & Simmons RM. (1977). Tension responses to sudden length change in stimulated frog muscle fibres near slack length. *J Physiol* **269,** 441-515.

Ford LE, Huxley AF & Simmons RM. (1981). The relation between stiffness and filament overlap in stimulated frog muscle fibres. *J Physiol* **311,** 219-249.

Fusi L, Brunello E, Reconditi M, Piazzesi G & Lombardi V. (2014). The non-linear elasticity of the muscle sarcomere and the compliance of myosin motors. *J Physiol* **592,** 1109-1118.

Geeves MA & Holmes KC. (2005). The molecular mechanism of muscle contraction. *Adv Protein Chem* **71,** 161-193.

Gilliver SF, Degens H, Rittweger J, Sargeant AJ & Jones DA. (2009). Variation in the determinants of power of chemically skinned human muscle fibres. *Exp Physiol* **94,** 1070-1078.

Goldman YE, Hibberd MG & Trentham DR. (1984). Initiation of active contraction by photogeneration of adenosine-5'-triphosphate in rabbit psoas muscle fibres. *J Physiol* **354,** 605-624.

Guth L & Samaha FJ. (1969). Qualitative differences between actomyosin ATPase of slow and fast mammalian muscle. *Exp Neurol* **25,** 138-152.

Han YS, Geiger PC, Cody MJ, Macken RL & Sieck GC. (2003). ATP consumption rate per cross bridge depends on myosin heavy chain isoform. *J Appl Physiol (1985)* **94,** 2188-2196.

He ZH, Bottinelli R, Pellegrino MA, Ferenczi MA & Reggiani C. (2000). ATP consumption and efficiency of human single muscle fibers with different myosin isoform composition. *Biophys J* **79,** 945-961.

Hill AV. (1938). The heat of shortening and the dynamic constants of muscle. *Proc R Soc Lond B Biol Sci* **126,** 136-195.

Holmes KC. (1997). The swinging lever-arm hypothesis of muscle contraction. *Curr Biol* **7,** R112-118.

Huxley AF. (1957). Muscle structure and theories of contraction. *Prog Biophys Biophys Chem* **7,** 255-318.

Huxley AF. (1974). Muscular contraction. *J Physiol* **243,** 1-43.

Huxley AF & Lombardi V. (1980). A sensitive force transducer with resonant-frequency 50 kHz. *J Physiol* **305,** 15-16.

Huxley AF, Lombardi V & Peachey D. (1981). A system for fast recording of longitudinal displacement of a striated muscle fibre. *J Physiol* **317,** 12-13.

Huxley AF & Simmons RM. (1971). Proposed mechanism of force generation in striated muscle. *Nature* **233,** 533-538.

Huxley HE, Reconditi M, Stewart A & Irving T. (2006). X-ray interference studies of crossbridge action in muscle contraction: evidence from quick releases. *J Mol Biol* **363,** 743-761.

Huxley HE, Stewart A, Sosa H & Irving T. (1994). X-ray diffraction measurements of the extensibility of actin and myosin filaments in contracting muscle. *Biophys J* **67,** 2411-2421.

Irving M, Piazzesi G, Lucii L, Sun YB, Harford JJ, Dobbie IM, Ferenczi MA, Reconditi M & Lombardi V. (2000). Conformation of the myosin motor during force generation in skeletal muscle. *Nat Struct Biol* **7,** 482-485.

Kabsch W, Mannherz HG, Suck D, Pai EF & Holmes KC. (1990). Atomic structure of the actin:DNase I complex. *Nature* **347,** 37-44.

Kawai M, Wray JS & Zhao Y. (1993). The effect of lattice spacing change on cross-bridge kinetics in chemically skinned rabbit psoas muscle fibers. I. Proportionality between the lattice spacing and the fiber width. *Biophys J* **64,** 187-196.

Kohler J, Winkler G, Schulte I, Scholz T, McKenna W, Brenner B & Kraft T. (2002). Mutation of the myosin converter domain alters cross-bridge elasticity. *Proc Natl Acad Sci U S A* **99,** 3557-3562.

LaFramboise WA, Daood MJ, Guthrie RD, Moretti P, Schiaffino S & Ontell M. (1990). Electrophoretic separation and immunological identification of type 2X myosin heavy chain in rat skeletal muscle. *Biochim Biophys Acta* **1035,** 109-112.

Linari M, Caremani M & Lombardi V. (2010). A kinetic model that explains the effect of inorganic phosphate on the mechanics and energetics of isometric contraction of fast skeletal muscle. *Proceedings of the Royal Society B-Biological Sciences* **277,** 19-27.

Linari M, Caremani M, Piperio C, Brandt P & Lombardi V. (2007). Stiffness and fraction of myosin motors responsible for active force in permeabilized muscle fibers from rabbit psoas. *Biophys J* **92,** 2476-2490.

Linari M, Dobbie I, Reconditi M, Koubassova N, Irving M, Piazzesi G & Lombardi V. (1998). The stiffness of skeletal muscle in isometric contraction and rigor: the fraction of myosin heads bound to actin. *Biophys J* **74,** 2459-2473.

Linari M, Piazzesi G & Lombardi V. (2009). The effect of myofilament compliance on kinetics of force generation by myosin motors in muscle. *Biophys J* **96,** 583-592.

Lombardi V & Piazzesi G. (1990). The contractile response during steady lengthening of stimulated frog muscle fibres. *J Physiol* **431,** 141-171.

Luff AR & Atwood HL. (1971). Changes in the sarcoplasmic reticulum and transverse tubular system of fast and slow skeletal muscles of the mouse during postnatal development. *J Cell Biol* **51,** 369-383.

Luther PK, Winkler H, Taylor K, Zoghbi ME, Craig R, Padron R, Squire JM & Liu J. (2011). Direct visualization of myosin-binding protein C bridging myosin and actin filaments in intact muscle. *Proc Natl Acad Sci U S A* **108,** 11423-11428.

Lymn RW & Taylor EW. (1971). Mechanism of adenosine triphosphate hydrolysis by actomyosin. *Biochemistry* **10,** 4617-4624.

Marston SB & Taylor EW. (1980). Comparison of the myosin and actomyosin ATPase mechanisms of the four types of vertebrate muscles. *J Mol Biol* **139,** 573-600.

Martyn DA, Chase PB, Regnier M & Gordon AM. (2002). A simple model with myofilament compliance predicts activation-dependent crossbridge kinetics in skinned skeletal fibers. *Biophys J* **83,** 3425-3434.

Matsubara I & Elliott GF. (1972). X-ray diffraction studies on skinned single fibres of frog skeletal muscle. *J Mol Biol* **72,** 657-669.

Maughan DW & Godt RE. (1979). Stretch and radial compression studies on relaxed skinned muscle fibers of the frog. *Biophys J* **28,** 391-402.

Millar NC & Homsher E. (1992). Kinetics of force generation and phosphate release in skinned rabbit soleus muscle fibers. *Am J Physiol* **262,** C1239-1245.

Mobley BA & Eisenberg BR. (1975). Sizes of components in frog skeletal muscle measured by methods of stereology. *J Gen Physiol* **66,** 31-45.

Needham DM. (1926). Red and white muscle. *Physiol Rev* **6,** 1-27.

Nyitrai M & Geeves MA. (2004). Adenosine diphosphate and strain sensitivity in myosin motors. *Philos Trans R Soc Lond B Biol Sci* **359,** 1867-1877.

Nyitrai M, Rossi R, Adamek N, Pellegrino MA, Bottinelli R & Geeves MA. (2006). What limits the velocity of fast-skeletal muscle contraction in mammals? *J Mol Biol* **355,** 432-442.

Park-Holohan S, Linari M, Reconditi M, Fusi L, Brunello E, Irving M, Dolfi M, Lombardi V, West TG, Curtin NA, Woledge RC & Piazzesi G. (2012). Mechanics of myosin function in white muscle fibres of the dogfish, Scyliorhinus canicula. *J Physiol* **590,** 1973-1988.

Pate E & Cooke R. (1989). Addition of phosphate to active muscle fibers probes actomyosin states within the powerstroke. *Pflugers Arch* **414,** 73-81.

Pellegrino MA, Canepari M, Rossi R, D'Antona G, Reggiani C & Bottinelli R. (2003). Orthologous myosin isoforms and scaling of shortening velocity with body size in mouse, rat, rabbit and human muscles. *J Physiol* **546,** 677-689.

Piazzesi G, Dolfi M, Brunello E, Fusi L, Reconditi M, Bianco P, Linari M & Lombardi V. (2014). The myofilament elasticity and its effect on kinetics of force generation by the myosin motor. *Arch Biochem Biophys* **552-553,** 108-116.

Piazzesi G & Lombardi V. (1995). A cross-bridge model that is able to explain mechanical and energetic properties of shortening muscle. *Biophys J* **68,** 1966-1979.

Piazzesi G, Lucii L & Lombardi V. (2002). The size and the speed of the working stroke of muscle myosin and its dependence on the force. *J Physiol* **545,** 145-151.

Piazzesi G, Reconditi M, Linari M, Lucii L, Bianco P, Brunello E, Decostre V, Stewart A, Gore DB, Irving TC, Irving M & Lombardi V. (2007). Skeletal muscle performance determined by modulation of number of myosin motors rather than motor force or stroke size. *Cell* **131,** 784-795.

Potma EJ & Stienen GJ. (1995). Influence of inorganic phosphate on ATP in fast and slow skeletal muscle fibers of the rabbit under the isometric conditions and during isovelocity shortenings. *Biophys J* **68,** 350s.

Potma EJ, van Graas IA & Stienen GJ. (1995). Influence of inorganic phosphate and pH on ATP utilization in fast and slow skeletal muscle fibers. *Biophys J* **69,** 2580-2589.

Rayment I, Holden HM, Whittaker M, Yohn CB, Lorenz M, Holmes KC & Milligan RA. (1993a). Structure of the actin-myosin complex and its implications for muscle contraction. *Science* **261,** 58-65.

Rayment I, Rypniewski WR, Schmidt-Base K, Smith R, Tomchick DR, Benning MM, Winkelmann DA, Wesenberg G & Holden HM. (1993b). Three-dimensional structure of myosin subfragment-1: a molecular motor. *Science* **261,** 50-58.

Reconditi M, Linari M, Lucii L, Stewart A, Sun YB, Boesecke P, Narayanan T, Fischetti RF, Irving T, Piazzesi G, Irving M & Lombardi V. (2004). The myosin motor in muscle generates a smaller and slower working stroke at higher load. *Nature* **428,** 578-581.

Reggiani C. (2007). When fibres go slack and cross bridges are free to run: a brilliant method to study kinetic properties of acto-myosin interaction. *J Physiol* **583,** 5-7.

Schiaffino S, Gorza L, Sartore S, Saggin L, Ausoni S, Vianello M, Gundersen K & Lomo T. (1989). Three myosin heavy chain isoforms in type 2 skeletal muscle fibres. *J Muscle Res Cell Motil* **10,** 197-205.

Schiaffino S, Hanzlikova V & Pierobon S. (1970). Relations between structure and function in rat skeletal muscle fibers. *J Cell Biol* **47,** 107-119.

Schiaffino S & Reggiani C. (2011). Fiber types in mammalian skeletal muscles. *Physiol Rev* **91,** 1447-1531.

Seebohm B, Matinmehr F, Kohler J, Francino A, Navarro-Lopez F, Perrot A, Ozcelik C, McKenna WJ, Brenner B & Kraft T. (2009). Cardiomyopathy mutations reveal variable region of myosin converter as major element of cross-bridge compliance. *Biophys J* **97,** 806-824.

Sellers JR. (1999). *Myosins*. Oxford University Press, New York.

Smith DA, Geeves MA, Sleep J & Mijailovich SM. (2008). Towards a unified theory of muscle contraction. I: foundations. *Ann Biomed Eng* **36,** 1624-1640.

Stephenson DG & Williams DA. (1982). Effects of sarcomere length on the force-pCa relation in fast- and slow-twitch skinned muscle fibres from the rat. *J Physiol* **333,** 637-653.

Talmadge RJ & Roy RR. (1993). Electrophoretic separation of rat skeletal muscle myosin heavy-chain isoforms. *J Appl Physiol (1985)* **75,** 2337-2340.

Thomas DD & Cooke R. (1980). Orientation of spin-labeled myosin heads in glycerinated muscle fibers. *Biophys J* **32,** 891-906.

Tikunov BA, Sweeney HL & Rome LC. (2001). Quantitative electrophoretic analysis of myosin heavy chains in single muscle fibers. *J Appl Physiol* **90,** 1927-1935.

Uyeda TQ, Abramson PD & Spudich JA. (1996). The neck region of the myosin motor domain acts as a lever arm to generate movement. *Proc Natl Acad Sci U S A* **93,** 4459-4464.

Wakabayashi K, Sugimoto Y, Tanaka H, Ueno Y, Takezawa Y & Amemiya Y. (1994). X-ray diffraction evidence for the extensibility of actin and myosin filaments during muscle contraction. *Biophys J* **67,** 2422-2435.

Walklate J, Ujfalusi Z & Geeves MA. (2016). Myosin isoforms and the mechanochemical cross-bridge cycle. *J Exp Biol* **219,** 168-174.

White HD & Taylor EW. (1976). Energetics and mechanism of actomyosin adenosine triphosphatase. *Biochemistry* **15,** 5818-5826.

Woledge RC. (1968). The energetics of tortoise muscle. *J Physiol* **197,** 685-707.

Zappe HA & Maeda Y. (1985). X-ray diffraction study of fast and slow mammalian skeletal muscle in the live relaxed state. *J Mol Biol* **185,** 211-214.